The condensate-forming protein eIF4ET ensures adequate levels of meiotic proteins to support oocyte storage

Priyankaa Bhatia[1], Judith Tafur[1], Ruchi Amin[2], Nicole E. Familiari[1], Kan Yaguchi[1], Vanna M. Tran[1], Alec Bond[1], Orhan Bukulmez[2], Jeffrey B. Woodruff[1,3]

1. Dept. of Cell Biology, Dept. of Biophysics, UT Southwestern Medical Center, Dallas, TX 75390, USA
2. Division of Reproductive Endocrinology and Infertility, Dept. of Obstetrics and Gynecology, UT Southwestern Medical Center Dallas, TX, USA
3. Correspondence to J. Woodruff: Jeffrey.woodruff@utsouthwestern.edu

ABSTRACT

Animals store oocytes in a dormant state for weeks to decades before ovulation. The homeostatic programs oocytes use to endure long-term storage are poorly understood. Using female nematodes as a short-lived model, we found that oocyte formation and storage required IFET-1, the conserved eIF4E-Transporter protein (eIF4ET). IFET-1 co-assembled with CAR-1 (Lsm14) to form micron-scale condensates in stored oocytes, which dissipated after oocyte activation. Depletion of IFET-1 destabilized the stored oocyte proteome, leading to lower translation, a decline in microtubule maintenance proteins, and errors in microtubule organization and meiotic spindle assembly. Deleting individual domains within IFET-1 impaired oocyte storage without affecting oocyte formation. Thus, in addition to establishing a healthy oocyte reserve in young mothers, IFET-1 ensures that correct levels of cytoskeletal proteins are maintained as oocytes age. Human eIF4ET also localized to micron-scale puncta in dormant oocytes in a reproductively healthy patient. Our results clarify the role for eIF4ET in maintaining the oocyte reserve and further support eIF4ET dysfunction as an upstream cause of embryonic aneuploidy and age-related infertility.

INTRODUCTION

The survival of many animal species depends on their ability to store high quality oocytes for prolonged periods of time. Such storage typically involves cell cycle arrest of the oocyte, typically in meiotic prophase I. In mammals, stored oocytes are small (~25-35 μm in diameter) and exist in a primordial follicle, where they are supported by squamous pre-granulosa cells (Gougeon, 1996; Li and Albertini, 2013). These oocytes can be reactivated to grow into immature GV oocytes (~100 μm in diameter), which then are either destroyed (atresia) or mature further into a metaphase-arrested form that is released for fertilization (ovulation) (Gougeon, 1996; Li and Albertini, 2013). A woman's pool of stored oocytes, called the ovarian reserve, declines immediately after birth, even before ovulation can occur. This decline continues as the woman ages, ultimately leading to a depleted ovarian reserve and menopause when she reaches 40-50 years of age (Hansen et al., 2008; Knowlton et al., 2014). Oocyte quality also decreases during long-term storage, as defined by an increase in mitochondrial dysfunction, DNA damage, and meiotic spindle errors (Gruhn et al., 2019; Hassold et al., 1980; Titus et al., 2013). These age-related errors are correlated with an increased risk of chromosomal abnormalities in the developing fetus and miscarriage (Nybo Andersen et al., 2000). Similar phenomena have been described in a wide variety of animals (Comizzoli and Ottinger, 2021). The confluence of declining oocyte numbers and quality are thus major contributors to age-related infertility in female mammals, yet the upstream molecular causes remain poorly understood.

While much research has revealed mechanisms of oocyte production, cell cycle arrest at the GV stage, and post-GV maturation (Li and Albertini, 2013; Pei et al., 2023), comparatively little is known about long-term oocyte maintenance. In preparation for storage, oocytes enter a state of cellular hibernation in part by reducing transcription and mitochondrial production of ATP (Moore et al., 1974; Rodriguez-Nuevo et al., 2022). Understanding storage requires identifying the molecules and mechanisms that continuously provide "life support" for the oocyte during its storage. A potential inroad is through studying a disease that affects oocyte storage. Primary Ovarian Insufficiency (POI) is characterized by an accelerated decline in the ovarian reserve or general dysfunction of ovarian follicles. Patients with POI typically experience irregular menstrual

61 cycles, low anti-Mullerian hormone, and premature menopause (26-32 years of
62 age)(Nelson, 2009). As these patients start out with a large ovarian reserve and can bear
63 children early (prior to menopause), this disease represents a case where the body fails
64 to preserve oocytes over time. Mutations in in Eukaryotic Translation Initiation Factor 4E
65 Nuclear Import Factor 1 (*EIF4ENIF1*), which encodes a protein from the conserved
66 eIF4ET family, are associated with POI, suggesting a link to oocyte quality control
67 (Kasippillai et al., 2013; Shang et al., 2022; Zhao et al., 2019). Consistent with this theory,
68 EIF4ENIF1 heterozygous knockout mice display reduced follicle pools and subfertility,
69 recapitulating key features of POI (Ding et al., 2023). In somatic tissue culture cells,
70 EIF4ENIF1 binds to and mediates nuclear import of the mRNA cap-binding protein eIF4E
71 (Dostie et al., 2000; Ferraiuolo et al., 2005; Kamenska et al., 2016). Through use of non-
72 natural reporters, these studies concluded that EIF4ENIF1 associates with P-bodies to
73 inhibit protein translation and stabilize mRNAs. Injection of EIF4ENIF1 into frog GV
74 oocytes also repressed translation of a luciferase reporter (Waghray et al., 2015).
75 EIF4ENIF1 is found in P-body-like granules in dormant mouse oocytes (Ding et al., 2023)
76 and in mitochondria-associated granules (MARDO) in mammalian GV oocytes (Cheng
77 et al., 2022). However, it is not known if EIF4ENIF1 is required specifically during oocyte
78 storage and if it regulates the global pool of natural mRNAs and proteins in that context.
79 The mechanism of oocyte storage remains poorly understood due to the difficulty in
80 accessing dormant oocytes. In mammals, dormant oocytes are obtained only through
81 invasive surgical resection of the ovarian cortex. *In vitro* gametogenesis also cannot be
82 used because it does not yet recapitulate formation and long-term maintenance of the
83 primordial follicle (McLaughlin et al., 2018), the fundamental storage unit that comprises
84 the dormant oocyte surrounded by pre-granulosa cells (Li and Albertini, 2013). Thus, it
85 is advantageous to use a genetic model organism with a short lifespan and oocytes that
86 are easily visualized *in situ*.
87 Here, we use *C. elegans* females to study oocyte maintenance mechanisms. Most
88 nematodes are gonochoric and store immature oocytes arrested in meiotic prophase I.
89 *C. elegans* is an outlier in that it recently evolved hermaphrodism, yet *C. elegans* females
90 retain the ability to store arrested oocytes in cases where sperm are depleted naturally or
91 genetically (*fog-2* or *fem-1* mutations)(Schedl and Kimble, 1988; Spence et al., 1990).

92 Thus, oocyte storage is an ancestral feature of nematodes. As *Caenorhabditis* species
93 live for several weeks and store their oocytes for less time, they represent an attractive
94 short-lived model for oocyte storage.
95
96 **RESULTS**
97
98 **Dysfunction of the eIF4ET homolog (IFET-1) impairs oocyte formation and storage**
99 **in female nematodes**
100 We developed an assay to test the effects of storage time on oocyte quality. We
101 generated a population of genetically identical *C. elegans* females through use of a
102 temperature-sensitive *fem-1(hc17)* loss-of-function allele. After synchronizing their
103 development, all worms reached adulthood and formed arrested oocytes at the same time
104 (first day of adulthood = Day 1). We then split the females into cohorts, letting them wait
105 another 1-5 days before introducing young males for mating. At the first day of mating
106 (Day 2), the female worms contained, on average, 34 +/- 7 oocytes (n= 20). Worms were
107 allowed to mate and lay fertilized eggs over 12-16 hr before removing all adults from the
108 plates. Since females can produce new oocytes after ovulating their stored oocytes, we
109 reported on worms that laid 34 or fewer eggs. After 2 days, we measured the number of
110 hatchlings divided by the number of eggs laid (oocyte viability) (Figure 1A). Under these
111 conditions, average oocyte viability declined with storage time, reaching 63.4% by day 6
112 (Figure 1B). From these data, we infer that *C. elegans* oocyte quality declines in
113 proportion to their storage time, like what is seen in mammals.
114 IFET-1 is the *C. elegans* homolog of EIF4ENIF1, but its role during oocyte storage
115 has not been tested. Full depletion of IFET-1 using RNAi rendered almost all stored
116 oocytes inviable (Figure 1B, S1A); IFET-1 levels remained low in stored oocytes, even
117 after worms were removed from the RNAi feeding plates (Figure S1B). IFET-1 depletion
118 also impaired ovulation in females and oocyte viability in hermaphrodites, which do not
119 arrest their oocytes, consistent with a previous study (Sengupta et al., 2013). Thus, full
120 knockdown of IFET-1 has pleiotropic effects making it difficult to assess its role
121 specifically during oocyte storage. Patients with EIF4ENIF1-linked primary ovarian
122 insufficiency (POI) all have heterozygous mutations, implying that failed oocyte storage

123 could be caused by partial reduction of EIF4ENIF1 activity. In our system, partial
124 knockdown of IFET-1 allowed young mothers to bear healthy progeny, although initial
125 viability was reduced to 31%. Oocyte viability declined faster than in controls, reaching
126 zero after 4 days of storage (Figure 1B). Oocytes in *ifet-1(RNAi)* females were irregular
127 in shape, as expected; however, all but the most proximal oocyte maintained arrest in
128 diakinesis, as indicated by the presence of intact germinal vesicles and condensed
129 chromosomes (Figure S1C). Thus, oocytes are still arrested in the absence of IFET-1,
130 but they are largely inviable. These results support previous findings that IFET-1 is
131 required for oocyte formation (Sengupta et al., 2013), and they further suggest that IFET-
132 1 could be required for maintenance of stored oocytes.

133 To definitively test the necessity of IFET-1 for the storage of healthy oocytes, we
134 sought a way to deplete IFET-1 only after oocyte formation is complete. Thus, we
135 generated a *fem-1* strain expressing a version of IFET-1 that is degraded by addition of
136 auxin (IFET-1::mScarlet::AID*). As outlined in Figure 1C, we placed synchronized adult
137 females which already have a row of arrested oocytes (Day 1) on plates with or without 4
138 mM auxin for 24 hr at 20°C. Then, we allowed worms to recover on normal NGM plates
139 for 8 hr at 20°C and allowed mating with males and egg laying for 12-16 hr at 16°C (Day
140 3). On average, worms laid 26 (control) vs. 13 (auxin) eggs during the laying period (n =
141 34 vs. 28 mothers, respectively); thus, any eggs or larvae on the plate derived from pre-
142 formed, healthy oocytes. Finally, we measured oocyte viability using the same method
143 described above.

144 Auxin treatment depleted IFET-1::mScarlet::AID* signal relative to controls (Figure
145 1D-E). In both cases, oocyte morphology appeared normal, suggesting that oocytes were
146 formed properly (Figure S1D). After 8 hr post-auxin removal, just prior to mating, IFET-1
147 signal did not recover within oocytes but did increase in the gonads (Figure S1E). Thus,
148 auxin-induced depletion of IFET-1::mScarlet::AID* in oocytes is robust and IFET-1 does
149 not re-accumulate in stored oocytes after auxin removal. Following mating, we observed
150 that auxin treatment significantly reduced oocyte viability (Figure 1F).

151 We considered the possibility that this phenotype could be due to IFET-1 being
152 essential during embryogenesis. However, treatment of excised embryos with 1 mM auxin
153 rapidly depleted IFET-1 but had no detectable effect on embryo development and viability

154 (Figure S1F,G). Auxin treatment did not significantly affect the fertility of control females
155 not expressing the degron, indicating that auxin is not generally toxic (Figure S1H). Thus,
156 the oocyte viability phenotype is due to lack of IFET-1 specifically during oocyte storage.
157 We conclude that IFET-1 is required to maintain oocyte quality during days-long storage.
158

159 **IFET-1 localizes to condensates that do not contain mitochondria**

160 To understand the function of IFET-1 in stored oocytes, we used confocal
161 microscopy to visualize IFET-1 tagged with mMaple (IFET-1::mMaple). Worms
162 expressing IFET-1::mMaple were viable and fertile (Figure S1I). In stored oocytes, IFET-
163 1::Maple localized to numerous micron-scale droplets, which we term condensates. After
164 activation of the oocytes through fertilization, these condensates dissolved and IFET-
165 1::Maple signal redistributed evenly throughout the oocyte cytoplasm (Figure 1G). A
166 similar behavior was reported for CAR-1, which localizes to droplets in stored oocytes
167 (Hubstenberger et al., 2013; Noble et al., 2008) and interacts with IFET-1 in embryo
168 extracts (Chen et al., 2016). To co-visualize CAR-1 and IFET-1, we tagged endogenous
169 CAR-1 at its C-terminus with mMaple and generated antibodies against both proteins for
170 immunofluorescence. CAR-1::mMaple localized to condensates in stored oocytes, as
171 expected, and co-localized with untagged IFET-1 (Figure 1H). IFET-1::mMaple also co-
172 localized with untagged CAR-1. RNAi depletion of IFET-1 reduced CAR-1 localization to
173 condensates (Figure 1I). These results indicate that IFET-1 and CAR-1 co-assemble into
174 supramolecular condensates in stored oocytes.

175 We wondered if the IFET-1/CAR-1 condensates function as Balbiani Bodies, which
176 are reported to encapsulate and confine mitochondria in the in dormant oocytes of
177 zebrafish, frogs, and humans (Boke et al., 2016; Hertig and Adams, 1967; Marlow and
178 Mullins, 2008). However, mitochondria are not spatially confined in stored *C. elegans*
179 oocytes (Bohnert and Kenyon, 2017), and we saw no significant co-localization between
180 HSP60 (mitochondria marker) and IFET-1 condensates (Figure 1J). We conclude that
181 IFET-1 condensates are not primitive Balbiani Bodies but rather a distinct class of protein-
182 based supramolecular assembly that exists in stored oocytes.
183

184 **Disrupting individual domains in IFET-1 perturbs oocyte storage but not formation**

185 We next tested which domains within IFET-1 are critical for its function in oocytes.
186 IFET-1 contains several conserved features: an eIF4E homology domain (Eif4EHD), Cup
187 Homology Domain (CHD), nuclear localization signal (NLS), a region rich in glutamines
188 (PolyQ), and a C-terminal coiled-coil (Figure 2A). We used CRISPR to delete each of
189 these regions in worms expressing endogenously tagged IFET-1::mMaple (Figure 2A).
190 We first analyzed homozygous mutant hermaphrodite worms, which make and activate
191 oocytes continuously with no storage phase (McCarter et al., 1999). In this condition, all
192 mutant worms produced viable oocytes; ΔCHD, ΔNLS, ΔPolyQ, mutants were nearly
193 identical to controls, while the ΔCoiledcoil mutant showed slightly reduced viability (Figure
194 2B).
195 Mutant female worms (ΔCHD, ΔNLS, ΔPolyQ, ΔCoiledcoil) formed oocytes with
196 proper cuboidal morphology but could not store them effectively: after two days of oocyte
197 storage followed by mating, embryo viability was reduced compared to eggs laid by age-
198 matched hermaphrodites (Figure 2B). IFET-1::mMaple mutants localized to condensates
199 in stored oocytes to differing degrees (Figure 2C,D). Mutants were expressed at 55-64%
200 of wild-type levels (Figure 2E). Importantly, for each mutant, expression levels were
201 similar between female worms with stored oocytes and hermaphrodites with non-stored
202 oocytes (Figure S2A,B); thus, the oocyte viability phenotype is due to a distinct role for
203 IFET-1 in storage that is not required during active oogenesis. We speculate that these
204 mutations comprise IFET-1 function, especially the ΔCHD mutation, which had the most
205 severe oocyte viability phenotype (21.8% viability after 2 days of storage) despite being
206 expressed at comparable levels to other mutants. The ΔCoiledcoil mutant had the largest
207 effect on condensate localization, suggesting that the coiled coil domain helps IFET-1 co-
208 assemble with CAR-1 to form condensates (Figure 2C). These results reveal that 1) IFET-
209 1 functions can be separated based on domains, and 2) multiple domains are required
210 for full-scale IFET-1 expression and function in stored oocytes. These data further support
211 our conclusion that IFET-1 is required to form oocytes and maintain their quality during
212 the storage phase.
213
214 **IFET-1 depletion causes imbalances in meiotic spindle protein levels**

215 To determine how IFET-1 dysfunction impacts oocyte quality, we performed
216 proteomic and transcriptomic analyses in control vs. *ifet-1(RNAi)* female worms
217 containing oocytes stored for 2 days. Since the majority of IFET-1 is expressed in the
218 germline (oocytes + syncytial gonad; Figure 1), we report data derived from whole worms
219 and follow up on specific hits with fluorescent reporters that are expressed in stored
220 oocytes.

221 Depletion of IFET-1 caused disruption of the proteome. Out of 3561 proteins
222 detected in both control and RNAi sets, 530 proteins (14.9%) were significantly
223 downregulated, while 100 proteins (2.8%) were significantly upregulated in *ifet-1(RNAi)*
224 worms (Figure 3A; Extended Data S1). IFET-1 levels were reduced to 15% of control
225 levels. This result contrasts with the expectation that IFET-1 functions as a broad scale
226 repressor, which was based on non-native reporter assays (Sengupta et al., 2013).
227 Transcriptomic analyses revealed few changes in mRNA levels in control vs. *ifet-1(RNAi)*
228 worms. Only 6.8% of all transcripts were significantly altered (4.5% up, 2.3% down) after
229 depletion of IFET-1 (Figure 3B; Extended Data S2). However, there was little overlap
230 between significant hits in the proteomic and transcriptomic data sets, suggesting that
231 proteomic changes largely did not result from changes in transcript levels (Figure S2A,
232 B).

233 Using Gene Ontology (GO) enrichment analysis of downregulated proteins in *ifet-*
234 *1(RNAi)* worms, we saw that the highest-ranking category included proteins related to
235 embryo development and egg hatching (Figure S3C; Extended Data Set 4). Within this
236 category were proteins required for meiotic spindle or microtubule function, such as
237 Katanin (MEI-1) and oocyte-specific isoforms of tubulin (TBA-1, TBA-2). Focusing on
238 meiotic spindle proteins, we also saw downregulation of Kinesin-like protein 15 (KLP-15),
239 TPX2 (TPXL-1), Dynein Light Intermediate Chain (DLI-1), Aurora A Kinase (AIR-1) and
240 other tubulin isoforms (TBB-1 and TBB-2) (Figure 3C). Not all microtubule-related
241 proteins were downregulated; for example, Dynein Heavy Chain (DHC-1), ch-TOG (ZYG-
242 9), and ASPM-1 were slightly upregulated. Levels of the transcripts encoding these
243 proteins were all slightly downregulated in *ifet-1(RNAi)* worms (60-95% of control; Figure
244 3D) and showed no correlation with proteomic changes (Figure 3E). Thus, IFET-1
245 regulates levels of meiotic spindle and microtubule-related proteins in a post-

246 transcriptional manner. Proteomic analysis also revealed lower MEI-1, AIR-1, DLI-1, and
247 TBB-1 levels in *ifet-1(ΔCHD)* mutant females, which are defective for oocyte storage and
248 not active oogenesis (Figure S3D).
249 We then analyzed global levels of translation using a SUnSET assay. Puromycin
250 incorporation was reduced in worms containing arrested oocytes vs. active oocytes
251 (Figure S3E); thus, reduced translation is a hallmark of oocyte storage in *C. elegans*.
252 Depletion of IFET-1 further reduced puromycin incorporation in stored oocytes (Figure
253 3F). Our results suggest that lowered meiotic protein levels in *ifet-1(RNAi)* female worms
254 are in part due to reduced translation.
255
256 **Loss of IFET-1 disrupts microtubule organization in stored and activated oocytes**
257 Our proteomic and transcriptomic data indicated that several meiotic spindle
258 proteins, but not their mRNAs, were downregulated in *ifet-1* mutants. We hypothesized
259 that such proteostatic dysfunction should affect meiotic progression, which could explain
260 how IFET-1 loss impairs oocyte viability. Thus, we generated feminized worms
261 expressing GFP-labeled beta tubulin (*fem-1*^{ts} GFP::TBB-2), allowed them to store
262 oocytes, then mated them with males to induce oocyte activation and meiotic spindle
263 assembly (Figure 4A). In control arrested oocytes (no RNAi), microtubules appeared
264 throughout the cytoplasm, but they concentrated in bright networks near the oocyte
265 periphery, as reported before (Harris et al., 2006). After oocytes were activated by mating,
266 the cytoplasmic microtubules disassembled, and the meiotic spindle formed (Figure 4B).
267 In *ifet-1(RNAi)* oocytes, GFP::TBB-2 did not localize to bright peripheral networks and
268 overall expression was lower, consistent with our proteomic data (Figure 4C,D). After
269 mating, bipolar formation of a single meiotic spindle per oocyte failed; instead, we
270 observed diminutive spindle-like structures, microtubule clusters, or aggregates of tubulin
271 signal (Figure 4C). Thus, IFET-1 is needed for organization of the microtubule
272 cytoskeleton during oocyte storage and resumption of meiosis.
273 Another protein affected by IFET-1 depletion was MEI-1/Katanin, a microtubule
274 severing enzyme important for meiotic spindle function (Yang et al., 2003). It is not known
275 if MEI-1 is made prior to oocyte formation, during oocyte storage, or in response to oocyte
276 activation. We thus used CRISPR to fuse MEI-1 with GFP (GFP::MEI-1) in feminized

worms. Confocal microscopy revealed GFP::MEI-1 signal was low in the syncytial gonad and increased 3.5-fold in stored oocytes (Figure 4E,F). GFP::MEI-1 signal was highest in the most proximal oocytes (i.e., the oldest). Thus, MEI-1 is translated in stored oocytes and accumulates over time. GFP::MEI-1 levels dropped dramatically after IFET-1 depletion (Figure 4E,F), consistent with our proteomic data. Treatment of adult worms with the proteasome inhibitor Bortezomib only weakly restored MEI-1::GFP levels in the oldest oocytes (Figure 4E,F). Overall, our results suggest that meiotic proteins are produced and maintained in stored oocytes through IFET-1-influenced translation and proteasome-mediated degradation. We conclude that IFET-1 ensures that stored oocytes produce the correct levels of MEI-1/Katanin, tubulin, and other proteins needed to organize the microtubule cytoskeleton and, after oocyte activation, to build a functional meiotic spindle.

The homolog of IFET-1 localizes to peri-nuclear puncta in dormant human oocytes

Our results suggest that IFET-1 plays an oocyte-intrinsic role in maintaining oocyte quality over time in *C. elegans*. We next examined the localization of the human homolog of IFET-1, called EIF4ENIF1. We surgically removed ovarian cortex strips from a reproductively healthy, 20-year-old patient (Figure 5A; see methods), and immediately fixed and processed the tissue for immunofluorescent staining. Stored oocytes reside in primordial follicles identified by a single layer of squamous pre-granulosa cells (Gougeon, 1996). Within these oocytes, EIF4ENIF1 localized to the cytoplasm and peri-nuclear, micron-scale puncta that morphologically resemble condensates (Figure 5B). EIF4ENIF1 puncta did not co-localize with mitochondria, similar to IFET-1 condensates in stored *C. elegans* oocytes (Figure 1). The EIF4ENIF1 puncta were specific to oocytes, as no significant signal was detected in the surrounding tissue (Figure 5C). We conclude that supramolecular assembly of eIF4ET family proteins into mitochondria-free condensates is a conserved feature of oocyte storage.

DISCUSSION

Diverse animals store and maintain immature eggs, called oocytes, for long periods of time before ovulating them. Here we used *C. elegans* females as a short-lived

308 model for oocyte storage and identified the eIF4ET family protein IFET-1 as essential for
309 oocyte formation and long-term maintenance. We report that in stored oocytes IFET-1
310 forms condensates and influences proteostasis, ensuring that Katanin, tubulin, and other
311 meiotic spindle proteins are maintained at the correct levels. This program ensures that
312 the oocyte microtubule cytoskeleton is supported during oocyte storage and then properly
313 reorganized into a functional meiotic spindle after oocyte activation.

314 Oocytes are thought to be largely translationally silent, yet they still produce
315 "houskeeping" proteins which are presumably needed for survival during long-term
316 storage (Richter and Lasko, 2011). Our data revealed that IFET-1 is needed for overall
317 translation in oocytes and, more specifically, achieving adequate levels housekeeping
318 proteins related to microtubule organization and completion of meiosis. IFET-1 co-
319 localized with CAR-1 (Lsm14B) in micron-scale condensates that formed in stored
320 oocytes but not in activated oocytes. Previous work suggested that these condensates
321 serve as super-stoichiometric repressor complexes that allow extreme concentration and
322 silencing of mRNAs (Cardona et al., 2023). If true, one would expect that dissolution of
323 the condensates would cause a massive upregulation of protein translation. IFET-1
324 depletion does increase expression of non-natural translational reporters (*gfp* fused to
325 different 3'UTRs)(Sengupta et al., 2013) and genes required for sperm production (e.g.,
326 *fog-1*, *daz-1*, *fem-3*)(Huggins et al., 2020). However, polysome profiling revealed that
327 translation is reduced in IFET-1-depleted hermaphrodites (Huggins et al., 2020). Our
328 SUNsET assay also showed reduced translation in *ifet-1(RNAi)* females containing stored
329 oocytes. These seemingly contradictory results are resolved by our unbiased proteomics:
330 530 proteins are significantly downregulated and 100 proteins are significantly
331 upregulated in *ifet-1(RNAi)* females. Thus, IFET-1 affects protein expression and stability
332 in a protein-specific manner. eIF4ET proteins are known to sequester eIF4E, thus
333 preventing interaction between the 40S ribosomal subunit and the 5' mRNA cap (Dostie
334 et al., 2000). By repressing translation of capped mRNAs, IFET-1 could, in theory, favor
335 translation of uncapped mRNAs needed for oocyte maintenance (Keiper, 2019). Why loss
336 of IFET-1 would lead to a decrease in global translation is still unclear. We also cannot
337 rule out the possibility that loss of select proteins is due to increased proteasome-
338 mediated degradation, which we showed is active for maintaining MEI-1 levels in stored

339 oocytes. The primary role of IFET-1 may also change in a cell-type-specific manner. Our
340 data, which used proteomics and live-cell imaging of GFP-tagged endogenous MEI-1,
341 clearly indicated that IFET-1 depletion reduces MEI-1 levels in stored oocytes. However,
342 a study using immunofluorescence reported higher levels of MEI-1 in the embryos of *ifet-*
343 *1* mutant hermaphrodites (Li et al., 2009). MEI-1 is normally degraded during the oocyte-
344 embryo transition (Kurz et al., 2002). It is possible that IFET-1 is required for both
345 translation of MEI-1 during oocyte storage and the factors that degrade MEI-1 during the
346 oocyte-embryo transition. Understanding the mechanistic link between IFET-1 and MEI-
347 1 translation will require future investigation. Our data revealed that many other classes
348 of proteins are affected by *ifet-1(RNAi)*; it is thus possible that IFET-1's control of MEI-1
349 and other microtubule-related protein levels is indirect.
350 IFET-1 shares homology to human EIF4ENIF1, a protein whose function during
351 mammalian oocyte storage remains poorly defined. Women with heterozygous mutations
352 in *EIF4ENIF1* suffer a form of early-onset infertility called Primary Ovarian Insufficiency
353 (POI)(Kasippillai et al., 2013; Shang et al., 2022; Zhao et al., 2019). Symptoms typically
354 arise in the patient's late 20's and early 30's and include amenorrhea, a rapid depletion
355 of the ovarian reserve of quiescent oocytes, and an elevated risk of miscarriage (Dean et
356 al., 2018). Prior to diagnosis, patients with POI can bear healthy children, indicating that
357 POI does not block or perturb oocyte development but rather the long-term maintenance
358 of oocytes in the ovary (Nelson, 2009). We showed that mutating conserved regions in
359 IFET-1 specifically impairs oocyte storage but not formation, thus mimicking a key feature
360 of POI. Furthermore, we demonstrated that EIF4ENIF1 localizes to micron-scale
361 condensates in dormant primary oocytes in a patient, similar to our observations of IFET-
362 1 in *C. elegans*. By analogy, it is possible that human oocytes assemble EIF4ENIF1
363 condensates or smaller cytoplasmic complexes as a quality control mechanism to
364 regulate protein levels during long-term oocyte storage. We hypothesize that EIF4ENIF1
365 dysregulation could be an upstream cause of meiotic division errors associated with age-
366 related infertility in women.
367
368 **ACKNOWLEDGEMENTS**

We thank the UTSW proteomics core facility for performing mass spectrometry, the UTSW Histology core for sectioning human tissue, and Abby Dernberg (UC Berkeley) for the mMaple plasmid.

FUNDING

This project was funded by a Pew Biomedical Scholars award, a Welch Catalyst award (V-I-0004-20230731), and the Endowed Scholars program at UT Southwestern (J.B.W). R.A and O.B are supported by an Obstetrics and Gynecology departmental fund.

AUTHOR CONTRIBUTIONS

P. Bhatia performed experiments in worms and analyzed data. J. Tafur performed the auxin-induced degradation experiments and analyzed data. N. Familiari maintained worms and performed crosses. V. Tran and A. Bond performed initial viability assays. K. Yaguchi made the GFP::MEI-1 strain. R. Amin performed the oophorectomy to retrieve human ovarian tissue and immunofluorescence. O. Bukulmez and J. Woodruff supervised the project. J. Woodruff wrote the paper.

SUPPLEMENTAL DATA

Figure S1. In vivo control experiments for oocyte proteins.

Figure S2. Analysis of *ifet-1* mutant worms.

Figure S2. Analysis of proteomic and transcriptomic data for female worms with stored oocytes.

Table S1. Table of *C. elegans* strains.

Extended Data Set 1. Protein abundances in control vs. *ifet-1(RNAi)* female worms with stored oocytes.

Extended Data Set 2. mRNA abundances in control vs. *ifet-1(RNAi)* female worms with stored oocytes.

Extended Data Set 3. Raw data for oocyte viability assays.

Extended Data Set 4. GO terms and protein classifications.

METHODS

400 **Worm Strains and Maintenance**

401 All worms were maintained at 16°C on Nematode Growth Media (NGM) with OP50 until
402 reaching the adult gravid stage and passaged regularly to maintain a steady population
403 of worms. GFP and mMaple knock-ins were generated using CRISPR (Paix et al.,
404 2015). Worm strains are listed in Table S1.

405

406 **Worm synchronization and feminization**

407 All worms with a fem-1 temperature sensitive genotype had to be maintained at 16ºC to
408 maintain hermaphrodites. When arrested oocytes were needed for an experiment, worms
409 were grown at 16ºC until the plate was full of mostly adults and eggs. Plates were washed
410 with 3.5ml of dH_2O and transferred to a falcon tube. To this, 1ml of 5% bleach and 0.5ml
411 of 5M NaOH was added and the falcon tubes spun for 1-2 minutes or until all adult worms
412 were dissolved. This embryo enriched solution was spun on a centrifuge at 1300 RCF for
413 1 min, then washed in DI water twice at same spin settings. The pellet of embryos was
414 resuspended in 1 ml of M9 media and left to rotate at room temperature overnight. The
415 next day, the tubes were collected and contained synchronized L1 hatchlings. These were
416 transferred to NGM plates with OP50 and grown at 25º for 72 hours to fully feminize and
417 mature to adults with oocytes in Day 1 arrest. It is at this stage that worms were collected
418 for all subsequent experiments.

419

420 **RNAi Knockdowns**

421 RNAi was done via feeding. The *ifet-1* clone was obtained from the [insert library here]
422 library and sequenced. The target sequence for ifet-1 is
423 AACGTGGCTAATCCAATGCTTGCAAGACTTTTCGGTCATAGTGGTGGTGATAACAA
424 CGCTTCATCTTCTGGAGCTGGTGATATAAAAGGAGGAATGCGGTTGGAAGATTTGG
425 AGAAAGGCATGGAGTCAAAGGAACCTTCAAAAGTCAGTCCATTGCAAGATCCATCA
426 CAACAAGCACAACTTCTGCAACATCTGCAAAAATTCGCCAAACAGCAAGCAGAGTC
427 TGGTCAGCACATACATCATCATAGACAACCAACACCACCAAATGGAGGTCCACAGC
428 ATCAACAACATTTGCATCACCCTATGGTTCATCCTGGAATGCAAATTATCGCAGATC
429 CAAGCCTTCTTGCAAGCTTCGCACAGAATCCAGTGATTTTGAATGCCTATGTCGAG
430 AATCAACTTCAAGAAGCAGTCAATGCTGCAATTCGTGCAAACAATGGGCAGCAGCT

431 TCCACCACAGCTTCGTATGTTAAGCATTTTTGAATACATTTCATGATTGAATTATTTT
432 TCAGATGAGCAACTTCGTATGGCATCCATGCGTAACAAGGCTTTCCTACAGTCTCA
433 GACTCTCACTTTCGTTAGTCTTCAACAACAGCATCAGAACATCCAGCAGCATCAGC
434 AACAACAACAGCATCATCAACACAAAGGTCGCACTCCTGCTATGATACCTGCGTCT
435 GTGCAGCGGCAATTGCAGAAGAGCTCCTCAAATGCTGATCAGAAGAAAGAAAAGA
436 CGAGTCAGAGCCCGCCAGAGAGCAACCAAGAGACTTCCGACGCTCATAATCAATC
437 TGATGCCATGAACCAACTGAAGAAATTGCACATGCAGCAGAACTATGCCAATATGG
438 TGCAGGCAATGAATTCTGGAGTCGGATGGGCACGCGGAAACGGCGTTGTTAACGG
439 ACAACAGCAACATCCACAGCAGCAACTTCCACCAAATGTTCAAATGCTGATGGCTC
440 AACACCAGCAAGCTCAAATGCAGCACCTCAAG.
441
442 Bacteria containing the target sequence plasmids were seeded onto NGM plates
443 containing 1mM IPTG and 100 ug/ml ampicillin. Worms were bleached and synchronized
444 as described above. After rotating overnight in M9, the L1 larvae were transferred onto
445 prepared RNAi plates and grown at 25ºC for 46-72 hours (depending on the experiment).
446 Worms were then transferred off the RNAi plate once they reached Day 1 of adulthood
447 and allowed to grow on OP50 at 20ºC.
448
449 **Auxin treatment**
450 Worm synchronization and feminization was conducted as described above. When
451 worms reached Day 1 of adulthood they were transferred to 20°C. Half the adult worms
452 were transferred to NGM plates with OP50 containing 4mM auxin for 24 hours, half were
453 maintained on a normal OP50 plate. After auxin treatment, the worms were transferred
454 back to a regular NGM plate with OP50 for 8 hours. Both control and auxin-treated worms
455 were then singled out to mate with 3 males for ~12-16 hours at 16°C. The males used
456 were also synchronized using the above method and grown to adulthood. At the end of
457 the mating period, adult worms were removed from the mating plates and the total amount
458 of embryos on each plate were counted. 2 days later the number of hatchlings on each
459 plate was counted and % embryonic viability was calculated. Data included was only
460 from worms that laid 34 or less embryos.
461

462 For IFET-1 depletion in embryos, embryos were extracted from IFET-1::mScarlet::AID*
463 hermaphrodite worms using two dissection needles in a solution of M9 containing 1 mM
464 auxin. These embryos were then imaged overnight on a Nikon Widefield microscope to
465 visualize hatching and IFET-1::mScarlet signal.
466
467 **Bortezomib Feeding**
468 Agar plates were prepared by diluting Bortezomib **(**Millipore Sigma, #5.04314**)** to 20 µM
469 in OP-50 and seeding plates as above. Worms were then fed on these plates for 16-24
470 hours to test recovery after RNAi feeding.
471
472 **Viability Assay**
473 Worms were bleached and synchronized as described above. L1 larvae were grown at
474 25ºC for 72 hours to feminize. After 72 hours, all adult worms on day 1 of oocyte arrest
475 were transferred to 20ºC to reduce heat stress and experiments were conducted on this
476 population. 12-15 day 2 adults were picked and transferred to individual mating plates.
477 f*og-2* worms were also synchronized and grown at the same rates and temperatures as
478 the feminized line. Three males per adult female were transferred to each mating plate.
479 Worms were allowed to mate and lay eggs for 10-16 hours at 16ºC. All adults were then
480 removed, and laid eggs were counted and recorded. 48 hours later, all hatchling larvae
481 were counted. Oocyte viability is calculated as number of hatchlings divided by the
482 number of eggs laid per mother. The average viability per strain is reported for worms
483 that laid ≤34 eggs to maintain a brood size that matches average oocyte storage numbers.
484
485
486 **Western Blot**
487 Worms were grown on agar plates until day 2 of adulthood. They were washed off the
488 plate with M9 and allowed to settle at the bottom of the tube. Worms were transferred
489 onto a fresh agar plate with no bacteria. 40 worms of each condition were picked and
490 transferred to 25 ul DI water. 25 µl SDS was added to the samples, and all were boiled at
491 95º for 5-10 minutes (or until worms dissolve). Samples were run on SDS-PAGE gel for
492 30 minutes. Proteins were transferred onto a nitrocellulose membrane using Trans Blot

493 Turbo Transfer System (Bio-Rad). Nitrocellulose was blocked in 3% blocking buffer for
494 an hour, then primary antibody (1:1000) was added for overnight incubation at 4ºC.
495 Membranes were washed the next morning in TBS-T three times, then incubated with
496 secondary antibody (1:10,000) for an hour. Membranes were washed again with TBS-T
497 three times and chemiluminescence was expressed using SuperSignal West Femto
498 Maximum Sensitivity Substrate (Thermo) Membranes were imaged on ChemiDoc Touch
499 Imaging System (Bio-Rad).
500 Quantification of western blots was calculated using FIJI. The mean gray value of any
501 protein bands of interest were measured and the background mean value of the blot was
502 subtracted. The mean gray value of the control was also measured in the same way
503 (whole lane was measured if it was a Ponceau S stain) and the values of the protein of
504 interest were normalized to the amounts of control or total protein stained.
505
506 **Collection, preparation, and staining of human ovarian tissue**
507 Tissue was collected as described (Amin et al., 2023). Briefly, a 20-year-old female
508 patient with no known pathology or history of infertility elected for total hysterectomy and
509 bilateral salpingo-oophorectomy for purposes of transgender care. Informed consent was
510 received prior to the procedure. Use of human ovarian tissue was approved by the
511 Institute Review Board of the University of Texas Southwestern Medical Center
512 (IRB#0801-404/012012-185). Ovarian tissue was placed in 4% formaldehyde directly
513 from the operating room and incubated for 24 hours for fixation. The tissue was embedded
514 in paraffin and cut into 5 mm sections using Leica Rotary Microtome. For
515 immunohistochemistry, the mounted paraffin sections were dewaxed and rehydrated in
516 xylene and serial dilutions of ethanol, respectively. Following a wash step with phosphate-
517 buffered solution (PBS), an antigen retrieval step was performed using a basic retrieval
518 reagent (R&D, CTS013, USA) at 90-95°C for 5 minutes. The slides were cooled
519 completely in PBS prior to processing.
520
521 For immunohistochemistry, the tissue was inserted into a solution containing 10% goat
522 serum, 3% bovine serum albumin, and 0.03% Triton X-100 (blocking solution) for one
523 hour. The tissue was then incubated overnight with primary antibody at 4°C. The following

524 primary antibodies were used: directly-labeled mouse monoclonal anti-HSP60
525 (Proteintech, 1:500 dilution; 66041-1-Ig, USA) and rabbit polyclonal anti-EIF4ENIF1
526 (Abcam, 1:500 dilution; ab277638, USA). After primary antibody incubation, a series of
527 washes were performed with PBS. The tissue was then incubated with a goat anti-rabbit
528 secondary antibody (Invitrogen, 1:1000 dilution, A-11008) for 1 hour prior to staining for
529 DNA with Vectashield (DAPI) (Vectorlabs, H-1000-10, USA). Negative controls were
530 included by incubating with no primary antibody. The directly labeled anti-HSP60 was
531 created using an Alexa Fluor 647 Lightning-Link kit (Abcam, USA) following their
532 instructions.
533
534 **Confocal microscopy**
535 Worms were imaged using a Nikon Eclipse Ti2-E microscope with a Yokogawa confocal
536 scanner unit (CSU-W1), piezo Z stage, and an iXon Ultra 888 EMCCD camera (Andor),
537 controlled by Nikon Elements software. Images were collected using a 60X water (NA
538 1.2) or 100X silicon (NA 1.35) immersion objective, 0.3 µm Z-stacks, 2x2 binning, 15%
539 laser power, and 100 ms exposures. Human tissue and worm oocytes were also imaged
540 using a Nikon AX-R confocal microscope with a 40X silicone (NA 1.25) objective.
541
542 **Proteomics**
543 Worms were feminized and synchronized as described above and plated on three
544 separate plates at 25ºC. When the worms reached Day 2 of adulthood, they were washed
545 in M9 media for 15 min to wash off bacteria. For each experimental group, three groups
546 of 30 worms each were collected and transferred to 20 µl of dH_2O in three separate
547 Eppendorf tubes. 20 µl SDS was added to the tubes and samples were boiled for 5-10
548 minutes (or until all worms were dissolved into SDS solution). These samples were run
549 on an SDS-PAGE gel for 3 min to allow all the sample to enter the gel, and then the gel
550 was stained with Coomassie dye. The protein band was cut out of the gel.
551
552 Gel samples were digested overnight with trypsin (Pierce) following reduction and
553 alkylation with DTT and iodoacetamide (Sigma–Aldrich). Following solid-phase extraction
554 cleanup with an Oasis HLB µelution plate (Waters), the resulting peptides were

555 reconstituted in 2% (v/v) acetonitrile (ACN) and 0.1% trifluoroacetic acid in water. 1 ug
556 of each sample was injected onto an Orbitrap Fusion Lumos mass spectrometer coupled
557 to an Ultimate 3000 RSLC-Nano liquid chromatography systems (Thermo). Samples were
558 injected onto a 75 µm i.d., 75-cm long EasySpray column (Thermo),and eluted with a
559 gradient from 0-28% buffer B over 90 min. Buffer A contained 2% (v/v) ACN and 0.1%
560 formic acid in water, and buffer B contained 80% (v/v) ACN, 10% (v/v) trifluoroethanol,
561 and 0.1% formic acid in water. The mass spectrometer operated in positive ion mode with
562 a source voltage of 2.5 kV and an ion transfer tube temperature of 300 °C. MS scans
563 were acquired at 120,000 resolution in the Orbitrap and up to 10 MS/MS spectra were
564 obtained in the Orbitrap for each full spectrum acquired using higher-energy collisional
565 dissociation (HCD) for ions with charges 2-7. Dynamic exclusion was set for 25 s after an
566 ion was selected for fragmentation.
567
568 Raw MS data files were analyzed using Proteome Discoverer v3.0 (Thermo), with peptide
569 identification performed using Sequest HT searching against the C. elegans reviewed
570 protein database from UniProt along with the sequence of fluorescent mMaple protein.
571 Fragment and precursor tolerances of 10 ppm and 0.6 Da were specified, and three
572 missed cleavages were allowed. Carbamidomethylation of Cys was set as a fixed
573 modification and oxidation of Met was set as a variable modification. The false-discovery
574 rate (FDR) cutoff was 1% for all peptides.
575
576 Data was analyzed in XMLS format. All protein abundances were normalized by
577 averaging the sum of total proteins in each sample sent and getting a ratio to the average
578 of the control samples sent. The ratios derived were used to adjust the protein abundance
579 values up or down accordingly. From these normalized values, the fold change and P-
580 value (2-tailed, unequal variance) were calculated. Anything with a p-value below 0.05
581 was deemed significant. Data was plotted using GraphPad Prism. Identified proteins are
582 listed in Extended Data Set 1. GO Term analysis was conducted using PANEGA
583 (https://www.flyrnai.org/tools/pangea/web/home/6239).
584
585 **Transcriptomics**

586 Worms were synchronized, feminized and grown on two 100 mm plates. When worms
587 reached day 2 of adulthood, they were washed off the plates with M9 and rotated for 20
588 min to remove all the bacteria. Worms were rinsed twice with M9. Total RNA was
589 extracted from worms with the Arcturus PicoPure RNA Isolation Kit (Applied
590 Biosystems™). Total RNA was shipped to Novogene (Sacramento, CA, USA). RNA
591 degradation and contamination was monitored on 1% agarose gels. RNA purity was
592 checked using the NanoPhotometer® spectrophotometer (IMPLEN, CA, USA). RNA
593 integrity and quantitation were assessed using the RNA Nano 6000 Assay Kit of the
594 Bioanalyzer 2100 system (Agilent Technologies, CA, USA).
595
596 A total amount of 1 μg RNA per sample was used as input material for the RNA sample
597 preparations. Sequencing libraries were generated using NEBNext® UltraTM RNA
598 Library Prep Kit for Illumina® (NEB, USA) following manufacturer's recommendations and
599 index codes were added to attribute sequences to each sample. Briefly, mRNA was
600 purified from total RNA using poly-T oligo-attached magnetic beads. Fragmentation was
601 carried out using divalent cations under elevated temperature in NEBNext First Strand
602 Synthesis Reaction Buffer (5X). First strand cDNA was synthesized using random
603 hexamer primer and M-MuLV Reverse Transcriptase (RNase H-). Second strand cDNA
604 synthesis was subsequently performed using DNA Polymerase I and RNase H.
605 Remaining overhangs were converted into blunt ends via exonuclease/polymerase
606 activities. After adenylation of 3' ends of DNAfragments, NEBNext Adaptor with hairpin
607 loop structure were ligated to prepare for hybridization. In order to select cDNA fragments
608 of preferentially 150~200 bp in length, the library fragments were purified with AMPure
609 XP system (Beckman Coulter, Beverly, USA). Then 3 μl USER Enzyme (NEB, USA) was
610 used with size-selected, adaptor-ligated cDNA at 37 °C for 15 min followed by 5 min at
611 95 °C before PCR. Then PCR was performed with PhusionHigh-Fidelity DNA polymerase,
612 Universal PCR primers and Index (X) Primer. PCR products were purified (AMPure XP
613 system) and library quality was assessed on the Agilent Bioanalyzer 2100 system.
614
615 The clustering of the index-coded samples was performed on a cBot Cluster Generation
616 System using PE Cluster Kit cBot-HS (Illumina) according to the manufacturer's

instructions. After cluster generation, the library preparations were sequenced on an Illumina platform and paired-end reads were generated. Raw data (raw reads) of FASTQ format were firstly processed through fastp. In this step, clean data (clean reads) were obtained by removing reads containing adapter and poly-N sequences and reads with low quality from raw data. At the same time, Q20, Q30 and GC content of the clean data were calculated. All the downstream analyses were based on the clean data with high quality.

Reference genome and gene model annotation files were downloaded from genome website browser (NCBI/UCSC/Ensembl) directly. Paired-end clean reads were aligned to the reference genome using the Spliced Transcripts Alignment to a Reference (STAR) software, which is based on a previously undescribed RNA-seq alignment algorithm that uses sequential maximum mappable seed search in uncompressed suffix arrays followed by seed clustering and stitching procedure. STAR exhibits better alignment precision and sensitivity than other RNA-seq aligners for both experimental and simulated data. Differential expression analysis between two conditions/groups (three biological replicates per condition) was performed using DESeq2 R package. DESeq2 provides statistical routines for determining differential expression in digital gene expression data using a model based on the negative binomial distribution. The resulting P values were adjusted using the Benjamini and Hochberg's approach for controlling the False Discovery Rate (FDR). Genes with an adjusted P value < 0.05 found by DESeq2 were assigned as differentially expressed.

Prior to differential gene expression analysis, for each sequenced library, the read counts were adjusted by Trimmed Mean of M-values (TMM) through one scaling normalized factor. Differential expression analysis of two conditions was performed using the edgeR R package. The P values were adjusted using the Benjamini and Hochberg methods. Corrected p value of 0.005 and |log2(Fold Change)| of 1 were set as the threshold for significantly differential expression. Identified transcripts are listed in Extended Data Set 2.

648 **Puromycin Assay**

649 Worms were synchronized and grown at 25º on 100mm NGM plates till they reached Day
650 2 of adulthood. They were washed off the plates with M9 buffer and rinsed in an
651 Eppendorf tube with S-Basal Medium (100mM NaCl, 5mM K_2HPO_4, 50mM KH_2PO_4,
652 5µg/ml cholesterol, 10mM potassium citrate, 3mM $MgSO_4$, 1% trace metals solution)
653 twice. 250µl of S-Basal Medium was added to the live worm pellet along with 50 µl of
654 10mg/ml puromycin, 200ul of concentrated OP50 and topped off to 1 ml with S-Basal
655 Medium. The tubes were shaken at 200rpm for 4 hours at room temperature. After 4
656 hours, tubes were collected, and the worms were washed with S-Basal three times.
657 Worms were resuspended in 300ul lysis buffer with Protease Inhibitors (150mM NaCl,
658 50mM Hepes, 1mM EDTA, 1% Triton-X, 0.5% SDS) and flash frozen in liquid nitrogen.
659 The tubes were placed on ice and sonicated 5-8 times at 20-30% amplitude for 2 seconds
660 at a time (until most carcasses were dissolved). They were then spun at 13,000 RPM for
661 30 mins and 300 µl of the supernatant was collected. 20% v/v of TCA was added to
662 solution and protein was allowed to precipitate for 30 min on ice. Tubes were spun at
663 14,000 RPM for 5 min and the supernatant was pipetted off. Pellet was washed twice in
664 90% acetone and then resuspended and boiled in 40 µl 2X SDS loading buffer. Samples
665 were run on an SDS-PAGE gel, transferred to nitrocellulose and first stained with
666 Ponceau-S stain and imaged. Membranes were then stained with anti-puromycin
667 antibody (Millipore Sigma, MABE343**)** and imaged using a ChemiDoc imager (Bio-Rad).

668

669 **Immunostaining of *C. elegans***

670 Tube fixation and collagenase protocol was adapted from protocols in
671 www.wormbook.org. Briefly, worms were fixed in 4% formaldehyde in PBS in an
672 eppendorf tube. Tubes were flash frozen in liquid nitrogen and subsequently thawed 2-3
673 times. They were shaken at 37ºC for 3 hours. Fixative was then removed and washed off
674 with PBST. Worms were shaken at 100rpm in B-mercaptoethanol solution (5%BME,
675 1%Triton X-100, 120 mM Tris) for 2 hours at 37º. Tubes were spun at 1000 RCF and
676 washed with PBST up to 10 times if needed, or until fixative is no longer detectable.
677 Samples were transferred to a fresh tube after half the washes. 200 µl of Collagenase
678 Solution (100 mM Tris, 1mM $CaCl_2$, 0.1%Triton X-100, pH 7.4, 2000 units Collagenase)

679 was added and worms were shaken at 37ºC at 250 rpm for 38-48 hours (depending on
680 the stock of collagenase). Incubation was stopped when a majority of worms were broken
681 in half. Collagenase was washed off and worms were blocked in 1 ml blocking buffer
682 (PBS, 0.5%Triton X-100, 1mM EDTA, 5%BSA, 0.05% Sodium Azide) at room
683 temperature for 1 hour. Blocking buffer was removed and worms were incubated with
684 primary antibody in blocking buffer (1:1000) overnight at 4ºC. Worms were washed three
685 times for 15-minute washes with antibody buffer (blocking buffer but with only 0.1% BSA)
686 and then incubated with secondary antibody in blocking buffer (1:10,000) for 3 hours at
687 room temperature. Three more 15-minute washes were done and worms transferred onto
688 a slide with an agar pad or wire-spacing. Mounting medium was added and slides were
689 imaged on spinning disc confocal. Rabbit polyclonal anti-IFET-1 and anti-CAR-1
690 antibodies were made by GenScript.
691
692 **Statistical analyses**
693 Statistical analyses were performed using GraphPad Prism. The indicated tests, the n
694 values, and significant values are displayed in the figure legends or on the figures
695 themselves. Significance was reported as: p value < 0.05 = *, p value < 0.005 = **, p
696 value < 0.0005 = ***, p value of < 0.00005 = ****.
697
698 **TABLE S1. *C. elegans* strains.**

Strain name	**genotype**	**Creation method**	**Origin**
BA17	*fem-1 (hc17) IV*	mutagenesis	CGC
CB4108	*fog-2(q71) V*	mutagenesis	CGC
JWW112	*car-1(utsw6[car-1::mMaple]) I*	CRISPR	This study
JWW166	*ifet-1(utsw15[ifet-1::mMaple]) III*	CRISPR	This study
JWW173	*utsw15[ifet-1::mMaple]III; fem-1 (hc17) IV*	cross	This study

JWW140	*car-1(utsw6[car-1::mMaple]) I; fem-1(hc17) IV*	cross	This study
JWW236	*mei-1(utsw17[gfp::mei-1]) I; fem-1 (hc17) IV*	CRISPR	This study
JWW163	*[pie-1p::GFP::H2B + unc-119(+)] III;fem-1 (hc17) IV*	cross	This study
PHX6862	*ifet-1(syb6862[ifet-1(Δ196-217)::mMaple]) III*	CRISPR	SunyBiotech
JWW228 (ΔCHD)	*ifet-1(syb6862[ifet-1(Δ196-217)::mMaple]) III; fem-1(hc17) IV*	cross	This study
PHX6949	*ifet-1(syb6949[ifet-1(Δ220-235)::mMaple]) III*	CRISPR	SunyBiotech
JWW215 (ΔNLS)	*ifet-1(syb6949[ifet-1(Δ220-235)::mMaple]) III; fem-1(hc17) IV*	cross	This study
PHX6886	*ifet-1(syb6862[ifet-1(Δ527-644)::mMaple]) III*	CRISPR	SunyBiotech
JWW216 (ΔpolyQ)	*ifet-1(syb6862[ifet-1(Δ527-644)::mMaple]) III; fem-1(hc17) IV*	cross	This study
PHX6954	*ifet-1(syb6862[ifet-1(Δ664-691)::mMaple]) III*	CRISPR	SunyBiotech
JWW230 (ΔCC)	*ifet-1(syb6862[ifet-1(Δ664-691)::mMaple]) III; fem-1(hc17) IV*	cross	This study
JWW252	*fem-1 (hc17) IV; ruls57[pie-1p::GFP::tubulin + unc-119(+)]*	cross	This study
JWW253	*ifet-1(utsw16[ifet-1::mScarlet_I::AID*::3xFlag]) III; wrdSi3 [sun-1p::TIR1::F2A::mTagBFP2::AID*::NLS::tbb-2 3'UTR] (II:0.77).*	CRISPR	This study
JWW255	*fem-1 (hc17) IV; ifet-1(utsw16[ifet-1::mScarlet_I::AID*::3xFlag]) III; wrdSi3 [sun-1p::TIR1::F2A::mTagBFP2::AID*::NLS::tbb-2 3'UTR] (II:0.77).*	cross	This study

REFERENCES

Amin, R., O. Bukulmez, and J.B. Woodruff. 2023. Visualization of Balbiani Body disassembly during human primordial follicle activation. *MicroPubl Biol*. 2023.

704 Bohnert, K.A., and C. Kenyon. 2017. A lysosomal switch triggers proteostasis renewal in the
705 immortal C. elegans germ lineage. *Nature*. 551:629-633.
706 Boke, E., M. Ruer, M. Wuhr, M. Coughlin, R. Lemaitre, S.P. Gygi, S. Alberti, D. Drechsel, A.A.
707 Hyman, and T.J. Mitchison. 2016. Amyloid-like Self-Assembly of a Cellular Compartment.
708 *Cell*. 166:637-650.
709 Cardona, A.H., S. Ecsedi, M. Khier, Z. Yi, A. Bahri, A. Ouertani, F. Valero, M. Labrosse, S. Rouquet,
710 S. Robert, A. Loubat, D. Adekunle, and A. Hubstenberger. 2023. Self-demixing of mRNA
711 copies buffers mRNA:mRNA and mRNA:regulator stoichiometries. *Cell*. 186:4310-4324
712 e4323.
713 Chen, J.X., P.G. Cipriani, D. Mecenas, J. Polanowska, F. Piano, K.C. Gunsalus, and M. Selbach.
714 2016. In Vivo Interaction Proteomics in Caenorhabditis elegans Embryos Provides New
715 Insights into P Granule Dynamics. *Mol Cell Proteomics*. 15:1642-1657.
716 Cheng, S., G. Altmeppen, C. So, L.M. Welp, S. Penir, T. Ruhwedel, K. Menelaou, K. Harasimov, A.
717 Stutzer, M. Blayney, K. Elder, W. Mobius, H. Urlaub, and M. Schuh. 2022. Mammalian
718 oocytes store mRNAs in a mitochondria-associated membraneless compartment.
719 *Science*. 378:eabq4835.
720 Comizzoli, P., and M.A. Ottinger. 2021. Understanding Reproductive Aging in Wildlife to Improve
721 Animal Conservation and Human Reproductive Health. *Front Cell Dev Biol*. 9:680471.
722 Dean, D.D., S. Agarwal, and P. Tripathi. 2018. Connecting links between genetic factors defining
723 ovarian reserve and recurrent miscarriages. *J Assist Reprod Genet*. 35:2121-2128.
724 Ding, Y., Z. He, Y. Sha, K. Kee, and L. Li. 2023. Eif4enif1 haploinsufficiency disrupts oocyte
725 mitochondrial dynamics and leads to subfertility. *Development*. 150.
726 Dostie, J., M. Ferraiuolo, A. Pause, S.A. Adam, and N. Sonenberg. 2000. A novel shuttling
727 protein, 4E-T, mediates the nuclear import of the mRNA 5' cap-binding protein, eIF4E.
728 *EMBO J*. 19:3142-3156.
729 Ferraiuolo, M.A., S. Basak, J. Dostie, E.L. Murray, D.R. Schoenberg, and N. Sonenberg. 2005. A
730 role for the eIF4E-binding protein 4E-T in P-body formation and mRNA decay. *J Cell Biol*.
731 170:913-924.
732 Gougeon, A. 1996. Regulation of ovarian follicular development in primates: facts and
733 hypotheses. *Endocr Rev*. 17:121-155.
734 Gruhn, J.R., A.P. Zielinska, V. Shukla, R. Blanshard, A. Capalbo, D. Cimadomo, D. Nikiforov, A.C.
735 Chan, L.J. Newnham, I. Vogel, C. Scarica, M. Krapchev, D. Taylor, S.G. Kristensen, J. Cheng,
736 E. Ernst, A.B. Bjorn, L.B. Colmorn, M. Blayney, K. Elder, J. Liss, G. Hartshorne, M.L.
737 Grondahl, L. Rienzi, F. Ubaldi, R. McCoy, K. Lukaszuk, C.Y. Andersen, M. Schuh, and E.R.
738 Hoffmann. 2019. Chromosome errors in human eggs shape natural fertility over
739 reproductive life span. *Science*. 365:1466-1469.
740 Hansen, K.R., N.S. Knowlton, A.C. Thyer, J.S. Charleston, M.R. Soules, and N.A. Klein. 2008. A
741 new model of reproductive aging: the decline in ovarian non-growing follicle number
742 from birth to menopause. *Hum Reprod*. 23:699-708.
743 Harris, J.E., J.A. Govindan, I. Yamamoto, J. Schwartz, I. Kaverina, and D. Greenstein. 2006. Major
744 sperm protein signaling promotes oocyte microtubule reorganization prior to
745 fertilization in Caenorhabditis elegans. *Dev Biol*. 299:105-121.
746 Hassold, T., P. Jacobs, J. Kline, Z. Stein, and D. Warburton. 1980. Effect of maternal age on
747 autosomal trisomies. *Ann Hum Genet*. 44:29-36.

748 Hertig, A.T., and E.C. Adams. 1967. Studies on the human oocyte and its follicle. I. Ultrastructural
749 and histochemical observations on the primordial follicle stage. *J Cell Biol*. 34:647-675.
750 Hubstenberger, A., S.L. Noble, C. Cameron, and T.C. Evans. 2013. Translation repressors, an RNA
751 helicase, and developmental cues control RNP phase transitions during early
752 development. *Dev Cell*. 27:161-173.
753 Huggins, H.P., J.S. Subash, H. Stoffel, M.A. Henderson, J.L. Hoffman, D.S. Buckner, M.S. Sengupta,
754 P.R. Boag, M.H. Lee, and B.D. Keiper. 2020. Distinct roles of two eIF4E isoforms in the
755 germline of Caenorhabditis elegans. *J Cell Sci*. 133.
756 Kamenska, A., C. Simpson, C. Vindry, H. Broomhead, M. Benard, M. Ernoult-Lange, B.P. Lee, L.W.
757 Harries, D. Weil, and N. Standart. 2016. The DDX6-4E-T interaction mediates
758 translational repression and P-body assembly. *Nucleic Acids Res*. 44:6318-6334.
759 Kasippillai, T., D.G. MacArthur, A. Kirby, B. Thomas, C.B. Lambalk, M.J. Daly, and C.K. Welt. 2013.
760 Mutations in eIF4ENIF1 are associated with primary ovarian insufficiency. *J Clin*
761 *Endocrinol Metab*. 98:E1534-1539.
762 Keiper, B.D. 2019. Cap-Independent mRNA Translation in Germ Cells. *Int J Mol Sci*. 20.
763 Knowlton, N.S., L.B. Craig, M.T. Zavy, and K.R. Hansen. 2014. Validation of the power model of
764 ovarian nongrowing follicle depletion associated with aging in women. *Fertil Steril*.
765 101:851-856.
766 Kurz, T., L. Pintard, J.H. Willis, D.R. Hamill, P. Gonczy, M. Peter, and B. Bowerman. 2002.
767 Cytoskeletal regulation by the Nedd8 ubiquitin-like protein modification pathway.
768 *Science*. 295:1294-1298.
769 Li, R., and D.F. Albertini. 2013. The road to maturation: somatic cell interaction and self-
770 organization of the mammalian oocyte. *Nat Rev Mol Cell Biol*. 14:141-152.
771 Li, W., L.R. DeBella, T. Guven-Ozkan, R. Lin, and L.S. Rose. 2009. An eIF4E-binding protein
772 regulates katanin protein levels in C. elegans embryos. *J Cell Biol*. 187:33-42.
773 Marlow, F.L., and M.C. Mullins. 2008. Bucky ball functions in Balbiani body assembly and animal-
774 vegetal polarity in the oocyte and follicle cell layer in zebrafish. *Dev Biol*. 321:40-50.
775 McCarter, J., B. Bartlett, T. Dang, and T. Schedl. 1999. On the control of oocyte meiotic
776 maturation and ovulation in Caenorhabditis elegans. *Dev Biol*. 205:111-128.
777 McLaughlin, M., D.F. Albertini, W.H.B. Wallace, R.A. Anderson, and E.E. Telfer. 2018. Metaphase
778 II oocytes from human unilaminar follicles grown in a multi-step culture system. *Mol*
779 *Hum Reprod*. 24:135-142.
780 Moore, G.P., S. Lintern-Moore, H. Peters, and M. Faber. 1974. RNA synthesis in the mouse
781 oocyte. *J Cell Biol*. 60:416-422.
782 Nelson, L.M. 2009. Clinical practice. Primary ovarian insufficiency. *N Engl J Med*. 360:606-614.
783 Noble, S.L., B.L. Allen, L.K. Goh, K. Nordick, and T.C. Evans. 2008. Maternal mRNAs are regulated
784 by diverse P body-related mRNP granules during early Caenorhabditis elegans
785 development. *J Cell Biol*. 182:559-572.
786 Nybo Andersen, A.M., J. Wohlfahrt, P. Christens, J. Olsen, and M. Melbye. 2000. Maternal age
787 and fetal loss: population based register linkage study. *BMJ*. 320:1708-1712.
788 Paix, A., A. Folkmann, D. Rasoloson, and G. Seydoux. 2015. High Efficiency, Homology-Directed
789 Genome Editing in Caenorhabditis elegans Using CRISPR-Cas9 Ribonucleoprotein
790 Complexes. *Genetics*. 201:47-54.

Pei, Z., K. Deng, C. Xu, and S. Zhang. 2023. The molecular regulatory mechanisms of meiotic arrest and resumption in Oocyte development and maturation. *Reprod Biol Endocrinol*. 21:90.

Richter, J.D., and P. Lasko. 2011. Translational control in oocyte development. *Cold Spring Harb Perspect Biol*. 3:a002758.

Rodriguez-Nuevo, A., A. Torres-Sanchez, J.M. Duran, C. De Guirior, M.A. Martinez-Zamora, and E. Boke. 2022. Oocytes maintain ROS-free mitochondrial metabolism by suppressing complex I. *Nature*. 607:756-761.

Schedl, T., and J. Kimble. 1988. fog-2, a germ-line-specific sex determination gene required for hermaphrodite spermatogenesis in Caenorhabditis elegans. *Genetics*. 119:43-61.

Sengupta, M.S., W.Y. Low, J.R. Patterson, H.M. Kim, A. Traven, T.H. Beilharz, M.P. Colaiacovo, J.A. Schisa, and P.R. Boag. 2013. ifet-1 is a broad-scale translational repressor required for normal P granule formation in C. elegans. *J Cell Sci*. 126:850-859.

Shang, L., S. Ren, X. Yang, F. Zhang, L. Jin, X. Zhang, and Y. Wu. 2022. EIF4ENIF1 variants in two patients with non-syndromic premature ovarian insufficiency. *Eur J Med Genet*. 65:104597.

Spence, A.M., A. Coulson, and J. Hodgkin. 1990. The product of fem-1, a nematode sex-determining gene, contains a motif found in cell cycle control proteins and receptors for cell-cell interactions. *Cell*. 60:981-990.

Titus, S., F. Li, R. Stobezki, K. Akula, E. Unsal, K. Jeong, M. Dickler, M. Robson, F. Moy, S. Goswami, and K. Oktay. 2013. Impairment of BRCA1-related DNA double-strand break repair leads to ovarian aging in mice and humans. *Sci Transl Med*. 5:172ra121.

Waghray, S., C. Williams, J.J. Coon, and M. Wickens. 2015. Xenopus CAF1 requires NOT1-mediated interaction with 4E-T to repress translation in vivo. *RNA*. 21:1335-1345.

Yang, H.Y., K. McNally, and F.J. McNally. 2003. MEI-1/katanin is required for translocation of the meiosis I spindle to the oocyte cortex in C elegans. *Dev Biol*. 260:245-259.

Zhao, M., F. Feng, C. Chu, W. Yue, and L. Li. 2019. A novel EIF4ENIF1 mutation associated with a diminished ovarian reserve and premature ovarian insufficiency identified by whole-exome sequencing. *J Ovarian Res*. 12:119.

822 **FIGURE LEGENDS**

823 **Figure 1: IFET-1 is required for long-term storage of quiescent oocytes in *C.***
824 ***elegans* females.**

825 A. Strategy to study oocyte storage and viability in *C. elegans* females. *fem-1(hc17)*
826 worms were synchronized at L1, grown to adulthood at 25°C to induce
827 feminization and oocyte storage, then separated into five different cohorts.
828 Female cohorts were mated with young males on different days, then offspring
829 were analyzed.
830 B. Percentage of oocytes that hatched, as described in A) (mean +/- 95% C.I. n=12-
831 30 worms, brood sizes ≤34 eggs laid). Partial knockdown of *ifet-1* was achieved
832 by feeding on RNAi plates for 48 hr; full knockdown was achieved by feeding for
833 72 hr. See Extended Data Set 3 for all viability data.
834 C. Strategy to deplete IFET-1 in stored oocytes after their formation. Synchronized
835 *fem-1(hc17) ifet-1::mScarlet::AID* TIR-1::T2A::BFP* adult female worms were
836 placed on plates with 0 mM or 4 mM auxin for 24 hr. Females were removed from
837 auxin for 8 hr prior to mating with males.
838 D. Left, diagram of a *C. elegans* female. Right, confocal image of Day 3 adult
839 females expressing IFET-1::mScarlet::AID* grown on plates containing 0 mM
840 (control) or 4 mM auxin. Scale Bar, 10µm
841 E. Integrated fluorescence intensity of IFET-1::mScarlet::AID* signal in stored
842 oocytes from panel D) (mean +/- 95% C.I.; n = 15 worms).
843 F. Viability of stored oocytes after mating in IFET-1::mScarlet worms with or without
844 auxin treatment (mean +/- 95% C.I.; n = 34 (control) vs. 28 (auxin) worms, brood
845 sizes =26 (control) vs 13 (auxin) eggs per mother).
846 G. Live-cell confocal images of IFET-1::mMaple in stored (female, not mated) and
847 activated (hermaphrodite) oocytes. Scale bars, 10 µm.
848 H. Immunofluorescence images of stored oocytes. Scale bars, 10 µm.
849 I. Left, images of stored oocytes expressing CAR-1::mMaple. Right, quantification
850 of total mass of CAR-1 condensates per worm (mean +/- 95% C.I. n = 850-900
851 condensates from 5-8 worms).

852 J. Immunofluorescent staining of mitochondria (HSP60) in stored oocytes
853 expressing IFET-1::mMaple. Scale bars, 10 μm.
854
855 **Figure 2. Specific domains in IFET-1 contribute to oocyte storage.**
856 A. Design of mutant constructs created with CRISPR modification of *ifet-1::mMaple*
857 worms. Shown is the protein sequence of IFET-1 (CHD, Cup Homology Domain;
858 NLS, nuclear localization signal; CC, coiled-coil domain; PolyQ, region rich in
859 glutamines).
860 B. Quantification of oocyte viability from 2-day-old adult hermaphrodites (Non-stored
861 oocytes) and females (Stored oocytes) after mating (mean +/- 95% C.I. n =
862 embryos from 15-22 worms, brood size ≤34 eggs laid for female worms). See
863 Extended Data Set 3 for raw data.
864 C. Confocal images of stored oocytes expressing the mutant variants of IFET-
865 1::mMaple shown in A.
866 D. Quantification of IFET-1::mMaple assembly into stored condensates (mean +/-
867 95% C.I. n = 500-600 condensates from 5-8 worms).
868 E. Quantification of mean IFET-1::mMaple fluorescence signal in oocytes (mean +/-
869 95% C.I. from 10-15 worms).
870
871 **Figure 3. Proteomic and transcriptomic profiling of oocyte-storing worms lacking**
872 **IFET-1.**
873 A. Left, volcano plot of protein abundance in *ifet-1(RNAi)* females vs. control
874 females. Right, pie chart indicating protein changes that surpassed significance
875 thresholds (p value < 0.05, fold change > 2; n = 3 replicates). See Extended Data
876 Set 1 for a list of all proteins.
877 B. Left, volcano plot of mRNA abundance in *ifet-1(RNAi)* females vs. control
878 females. Right, pie chart indicating protein changes that surpassed significance
879 thresholds (p value < 0.05, fold change > 2; n = 3 replicates). See Extended Data
880 Set 2 for a list of all transcripts.
881 C. Analysis of selected proteins related to meiotic spindle formation. Shown are
882 average protein abundances in *ifet-1(RNAi)* worms relative to controls.

883 D. Analysis of selected transcripts related to meiotic spindle formation. Shown are
884 average mRNA abundances in *ifet-1(RNAi)* worms relative to controls.
885 E. Comparison of changes in protein and mRNA abundance for genes/proteins
886 listed in C) and D). There is no correlation between the data sets (R^2= 0.007; n =
887 21).
888 F. SuNSET assay testing translation levels by measuring puromycin incorporation
889 into proteins. Lane 1, control female worms with stored oocytes. Lane 2, *ifet-*
890 *1(RNAi)* female worms with stored oocytes. Left, blot probing for puromycin.
891 Middle, ponceau stain showing total protein levels per sample. Right,
892 quantification of puromycin signal relative to ponceau signal and normalized to
893 signal of control worms. (n=4 blots).
894
895 **Figure 4. IFET-1 depletion affects organization of the microtubule cytoskeleton**
896 **and MEI-1/Katanin levels in stored oocytes.**
897 A. Workflow of experiments in female worms with stored oocytes. Mating induces
898 oocyte activation and meiotic spindle assembly.
899 B. Live-cell confocal images of arrested, activated, and Meiosis I oocytes in control
900 female worms expressing GFP::TBB-2 (beta tubulin). Yellow arrowhead, an
901 assembling meiotic spindle.
902 C. Same as in B), except with *ifet-1(RNAi)* female worms. Yellow arrowhead,
903 microtubule asters; Red arrowheads, tubulin aggregates.
904 D. Quantification of GFP::TBB-2 levels in arrested oocytes (mean +/- 95% C.I. n =
905 4-6 worms;).
906 E. Quantification of GFP::MEI-1 (Katanin) levels in arrested oocytes relative to
907 gonads (mean +/- 95% C.I. n = 6-8 worms;).
908 F. Images of GFP::MEI-1 expression in arrested oocytes. Top: Arrested oocytes,
909 Middle: arrested oocytes with *ifet-1(RNAi),* Bottom: arrested oocytes fed on *ifet-*
910 *1(RNAi)* and then on Bortezomib plates to block the proteosome. Scale bars= 10
911 µm.
912
913 **Figure 5. Localization of the IFET-1 homolog EIF4ENIF1 in human stored oocytes.**

914 A. H&E staining of an ovarian cortical slice resected from a 20-year-old patient.
915 Primordial follicles containing stored oocytes are labeled.
916 B. Immunofluorescent staining of mitochondria (HSP60), DNA, and EIF4ENIF1 in a
917 primordial follicle.
918 C. A larger view of the ovary cortex reveals that EIF4ENIF1 only localized to
919 oocytes within the primordial follicle and not surrounding cells.
920
921 **SUPPLEMENTAL FIGURE LEGENDS**
922 **Figure S1. In vivo control experiments for oocyte proteins.**
923 A. Western blot against IFET-1; anti-alpha tubulin blotting was used as a loading
924 control. Worm lysates were separated first by SDS-PAGE.
925 B. Confocal images of stored oocytes expressing IFET-1::mMaple with and without
926 *ifet-1(RNAi)* treatment across day 2 and day 5 of adulthood. Scale bars, 10 μm.
927 C. Confocal imaging of GFP-labeled histone H2B in stored oocytes (outlined in
928 dashed white lines). Scale bar, 10 μm.
929 D. DIC images of stored oocytes from the experiment in Figure 1 D-F. Scale bar, 10
930 μm.
931 E. Images of IFET-1::mScarlet::AID* signal in various conditions, related to Figure
932 1C-D.
933 F. Embryos were dissected in M9 + 1mM auxin and imaged with DIC (top) and
934 fluorescence (bottom) over time. Scale bar, 10 μm.
935 G. Viability of embryos after auxin treatment in panel F.
936 H. Viability of oocytes in *fem-1* worms not expressing a degron-tagged version of
937 IFET-1 (mean +/- 95% C.I.; n = 27 mothers, <34 laid eggs each). See Extended
938 Data Set 3 for raw data.
939 I. Viability of embryos laid by hermaphrodite versions of CRISPR-tagged strains
940 (mean +/- 95% C.I.; n = 12 mothers, >45 embryos each).
941
942 **Figure S2. Analysis of IFET-1 mutant worms.**
943 A. Western blot against IFET-1 in indicated strains. Hermaphrodite and female
944 worms indicated with symbols. Ponceau stain was used as a loading control.

945 B. Quantification of A) indicating grey values of IFET-1 in the western blot,
946 normalized by level of ponceau staining.
947
948 **Figure S3. Analysis of proteomic and transcriptomic data for female worms with**
949 **stored oocytes.**
950 A. Overlap between proteomic and transcriptomic data sets from Figure 3.
951 B. A list of the 15 gene products where mRNA and protein are significantly down-
952 regulated after RNAi against *ifet-1*.
953 C. GO-Term analysis of proteomic data in Figure 3.
954 D. Analysis of selected proteins related to meiotic spindle formation. Shown are
955 average protein abundances in *ifet-1(ΔCHD)* worms relative to *ifet-1(WT)*
956 controls. Bars indicate means (N= 2 data sets with 3 replicates each). Purple,
957 striped, and grey, indicate that the differences were significant in 2, 1, or 0 data
958 sets, respectively.
959 E. SUnSET assay comparing puromycin incorporation between worms with
960 activated oocytes and worms with arrested oocytes. Quantification of three blots
961 with arrested signal normalized to activated oocyte signal. (Significance tested
962 with one-sample t-test).

Figure 1

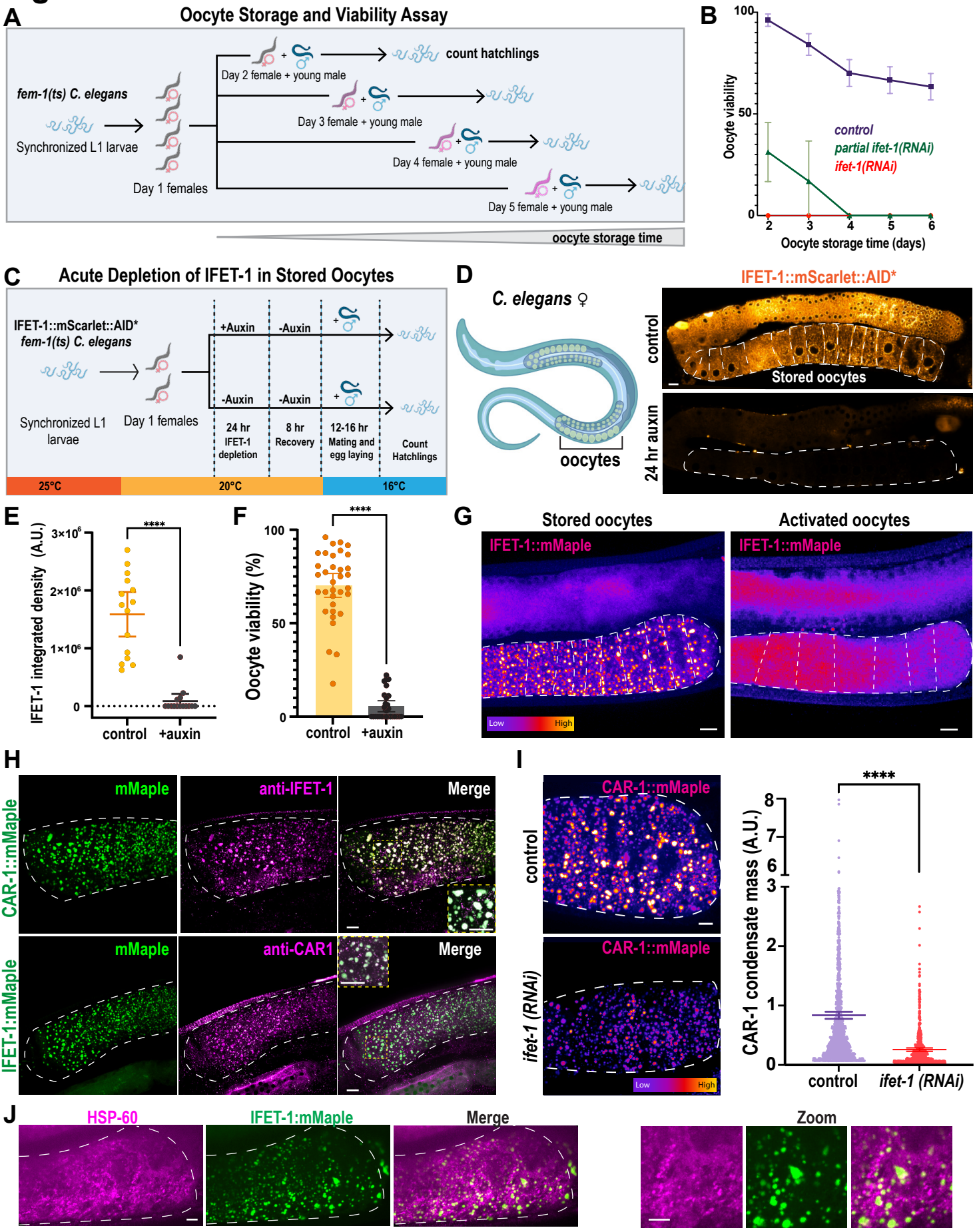
A
Oocyte Storage and Viability Assay
fem-1(ts) C. elegans
Synchronized L1 larvae
Day 1 females
Day 2 female + young male
count hatchlings
Day 3 female + young male
Day 4 female + young male
Day 5 female + young male
oocyte storage time
B
Oocyte viability
Oocyte storage time (days)
control
partial ifet-1(RNAi)
ifet-1(RNAi)
C
Acute Depletion of IFET-1 in Stored Oocytes
IFET-1::mScarlet::AID*
fem-1(ts) C. elegans
Synchronized L1 larvae
Day 1 females
+Auxin
-Auxin
24 hr IFET-1 depletion
8 hr Recovery
12-16 hr Mating and egg laying
Count Hatchlings
25°C
20°C
16°C
D
C. elegans ♀
oocytes
IFET-1::mScarlet::AID*
control
24 hr auxin
Stored oocytes
E
IFET-1 integrated density (A.U.)
control
+auxin
F
Oocyte viability (%)
control
+auxin
G
Stored oocytes
Activated oocytes
IFET-1::mMaple
Low
High
H
CAR-1::mMaple
IFET-1:mMaple
mMaple
anti-IFET-1
Merge
anti-CAR1
I
control
ifet-1 (RNAi)
CAR-1::mMaple
CAR-1 condensate mass (A.U.)
control
ifet-1 (RNAi)
J
HSP-60
IFET-1:mMaple
Merge
Zoom

Figure 2

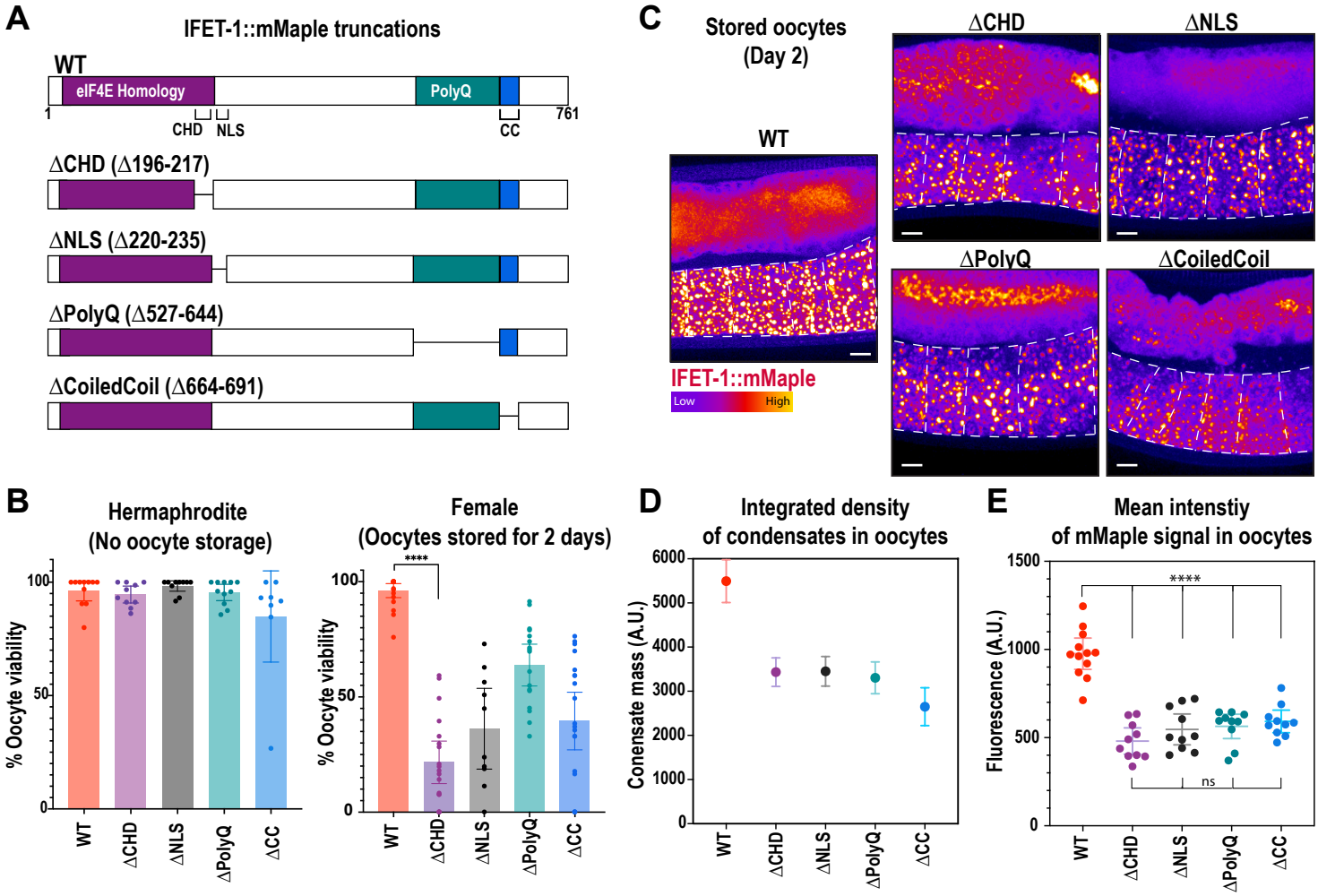
A
IFET-1::mMaple truncations
WT
eIF4E Homology
PolyQ
1
761
CHD
NLS
CC
ΔCHD (Δ196-217)
ΔNLS (Δ220-235)
ΔPolyQ (Δ527-644)
ΔCoiledCoil (Δ664-691)
C
Stored oocytes
(Day 2)
WT
ΔCHD
ΔNLS
ΔPolyQ
ΔCoiledCoil
IFET-1::mMaple
Low
High
B
Hermaphrodite
(No oocyte storage)
Female
(Oocytes stored for 2 days)
% Oocyte viability
****
D
Integrated density
of condensates in oocytes
Conensate mass (A.U.)
E
Mean intenstiy
of mMaple signal in oocytes
Fluorescence (A.U.)
ns

Figure 3

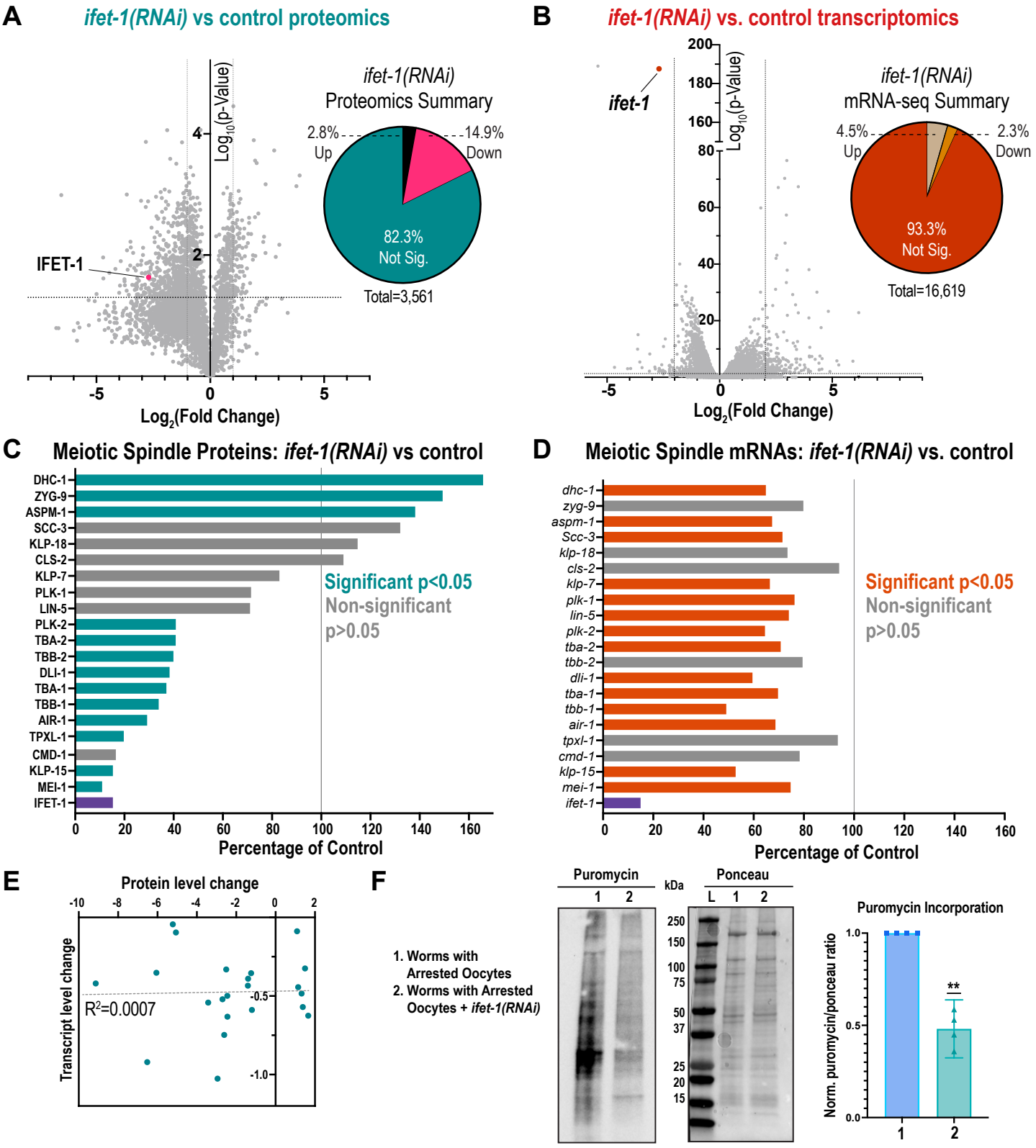
A
ifet-1(RNAi) vs control proteomics
IFET-1
Log10(p-Value)
Log2(Fold Change)
ifet-1(RNAi)
Proteomics Summary
2.8% Up
14.9% Down
82.3% Not Sig.
Total=3,561
B
ifet-1(RNAi) vs. control transcriptomics
ifet-1
Log10(p-Value)
Log2(Fold Change)
ifet-1(RNAi)
mRNA-seq Summary
4.5% Up
2.3% Down
93.3% Not Sig.
Total=16,619
C
Meiotic Spindle Proteins: ifet-1(RNAi) vs control
DHC-1
ZYG-9
ASPM-1
SCC-3
KLP-18
CLS-2
KLP-7
PLK-1
LIN-5
PLK-2
TBA-2
TBB-2
DLI-1
TBA-1
TBB-1
AIR-1
TPXL-1
CMD-1
KLP-15
MEI-1
IFET-1
Significant p<0.05
Non-significant p>0.05
Percentage of Control
D
Meiotic Spindle mRNAs: ifet-1(RNAi) vs. control
dhc-1
zyg-9
aspm-1
Scc-3
klp-18
cls-2
klp-7
plk-1
lin-5
plk-2
tba-2
tbb-2
dli-1
tba-1
tbb-1
air-1
tpxl-1
cmd-1
klp-15
mei-1
ifet-1
Significant p<0.05
Non-significant p>0.05
Percentage of Control
E
Protein level change
Transcript level change
R2=0.0007
F
1. Worms with Arrested Oocytes
2. Worms with Arrested Oocytes + ifet-1(RNAi)
Puromycin
Ponceau
kDa
L
Puromycin Incorporation
Norm. puromycin/ponceau ratio
**

Figure 4

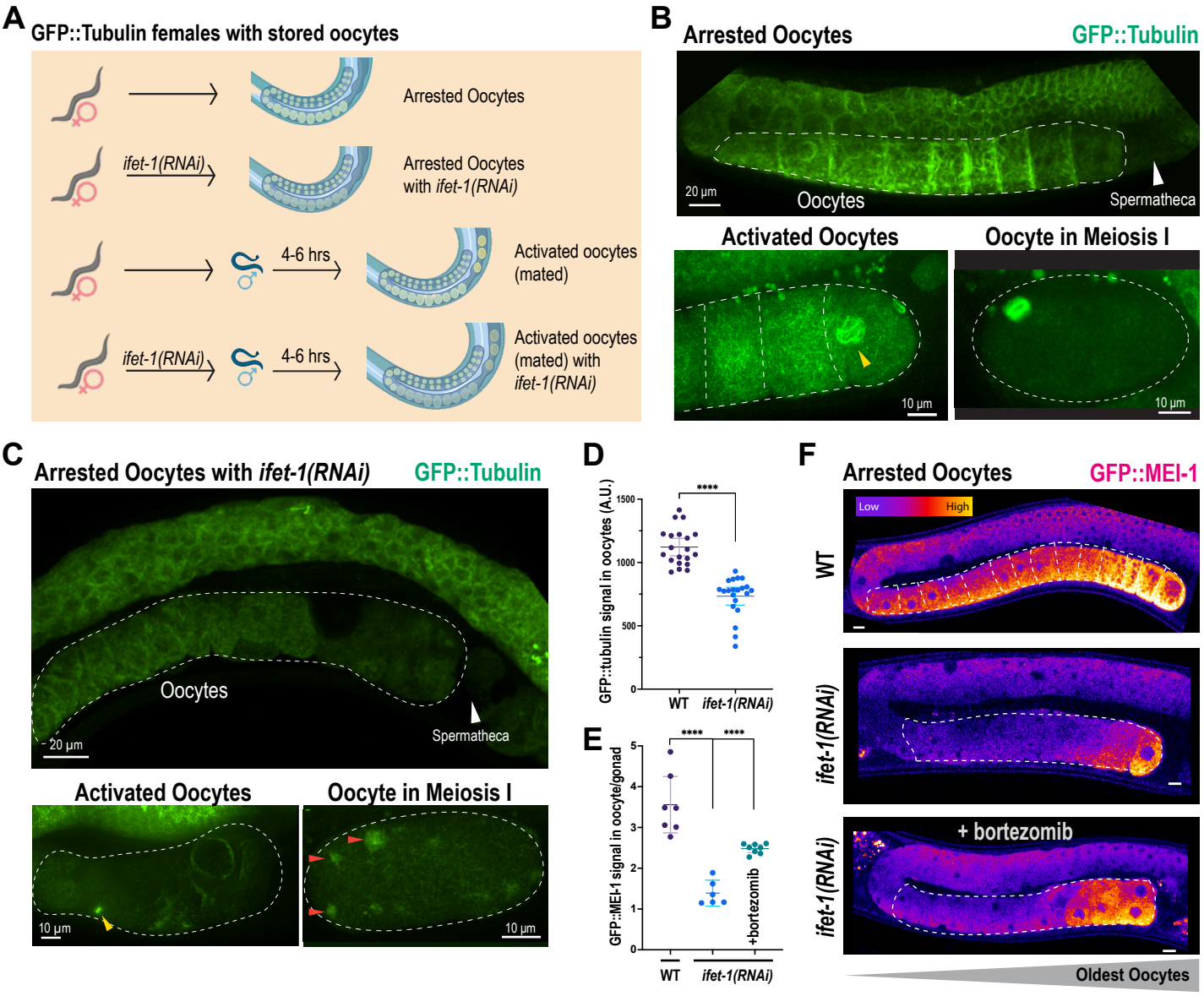
A
GFP::Tubulin females with stored oocytes
Arrested Oocytes
ifet-1(RNAi)
Arrested Oocytes with ifet-1(RNAi)
4-6 hrs
Activated oocytes (mated)
ifet-1(RNAi)
4-6 hrs
Activated oocytes (mated) with ifet-1(RNAi)
B
Arrested Oocytes
GFP::Tubulin
20 µm
Oocytes
Spermatheca
Activated Oocytes
Oocyte in Meiosis I
10 µm
10 µm
C
Arrested Oocytes with ifet-1(RNAi)
GFP::Tubulin
Oocytes
20 µm
Spermatheca
Activated Oocytes
Oocyte in Meiosis I
10 µm
10 µm
D
GFP::tubulin signal in oocytes (A.U.)
1500
1000
500
0
****
WT
ifet-1(RNAi)
E
GFP::MEI-1 signal in oocyte/gonad
5
4
3
2
1
0
****
****
+bortezomib
WT
ifet-1(RNAi)
F
Arrested Oocytes
GFP::MEI-1
Low
High
WT
ifet-1(RNAi)
ifet-1(RNAi)
+ bortezomib
Oldest Oocytes

Figure 5

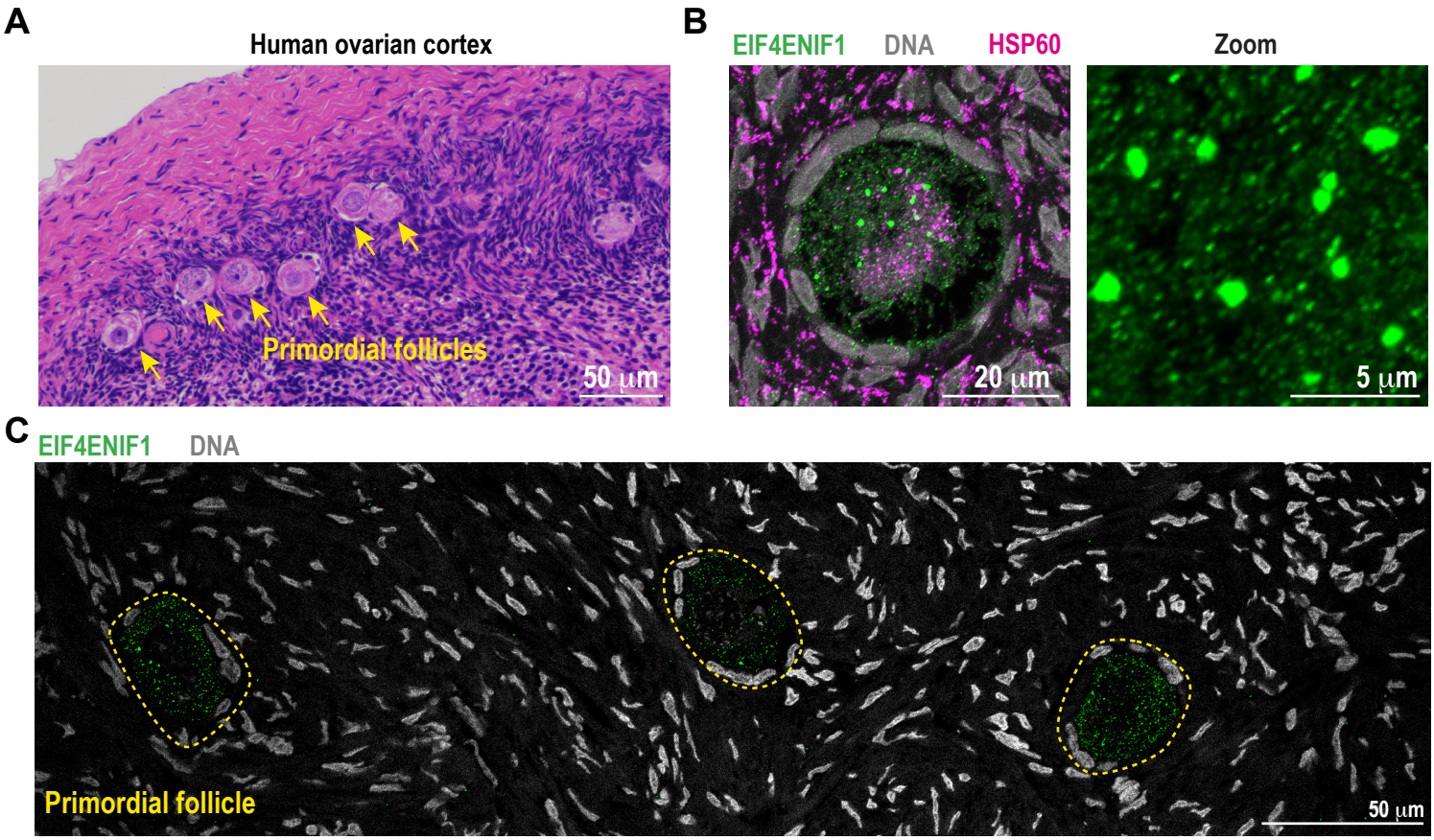
A
Human ovarian cortex
Primordial follicles
50 μm
B
EIF4ENIF1
DNA
HSP60
Zoom
20 μm
5 μm
C
EIF4ENIF1
DNA
Primordial follicle
50 μm

Figure S1

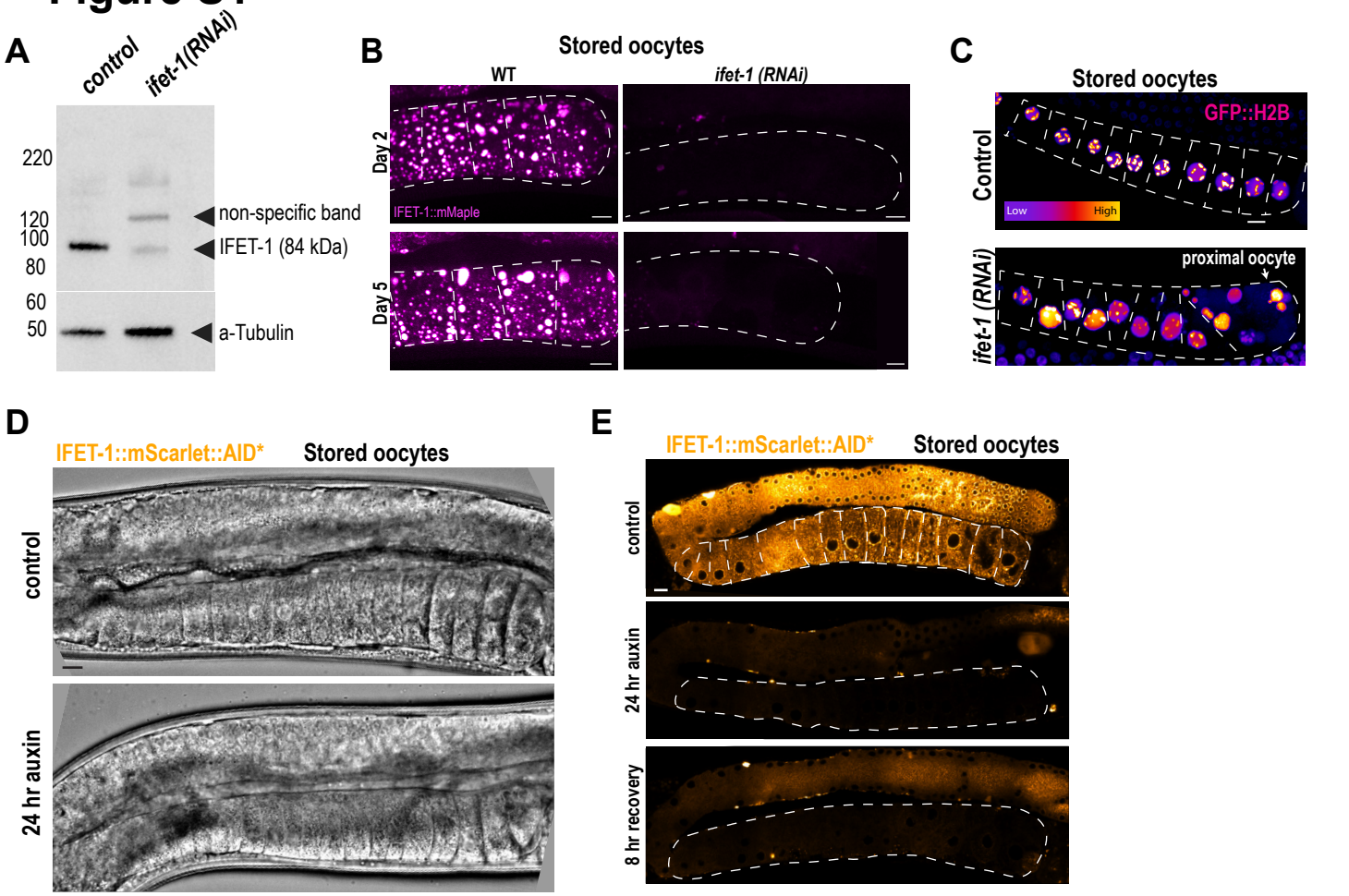

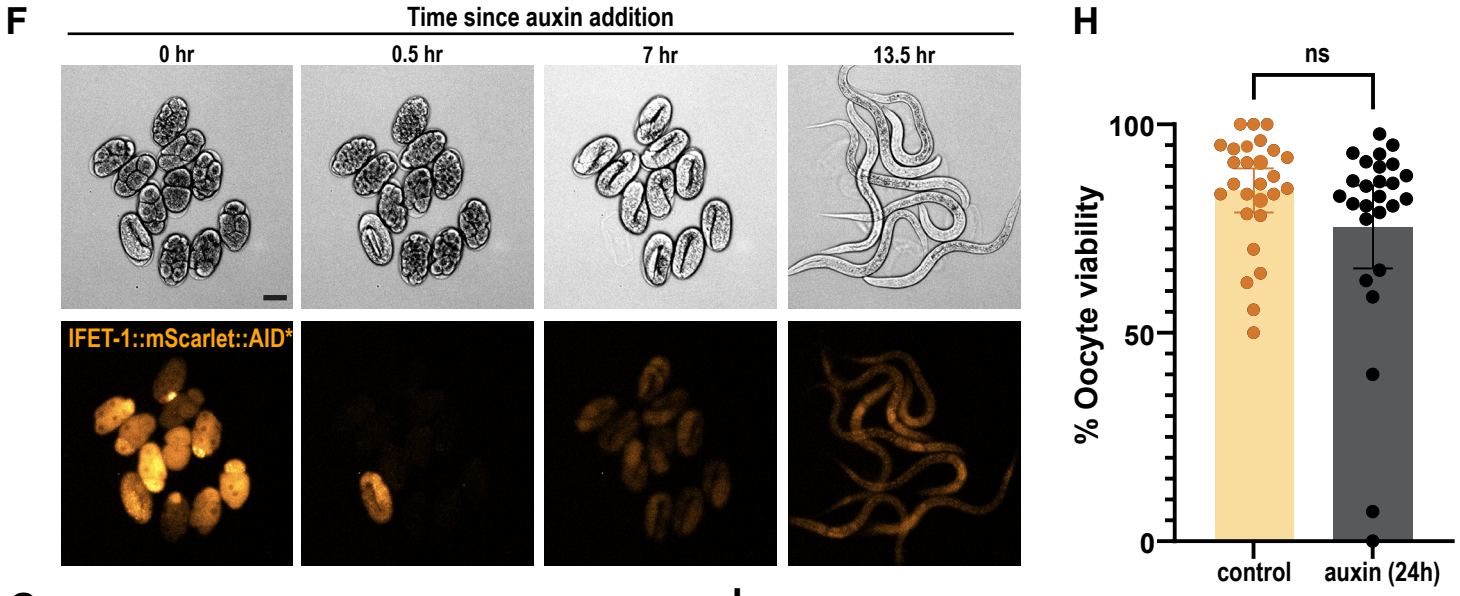

G

Embryo Stage	Embryos	Hatchlings	% Viability
1-cell	8	8	100
2-cell	22	20	90.5
4-cell	17	17	100
8-cell	15	14	92.3
Total	62	59	95.7

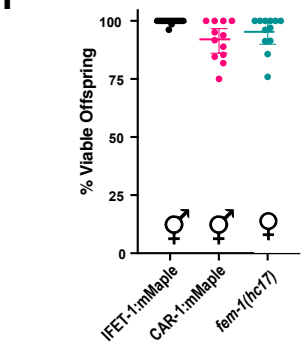

Figure S2

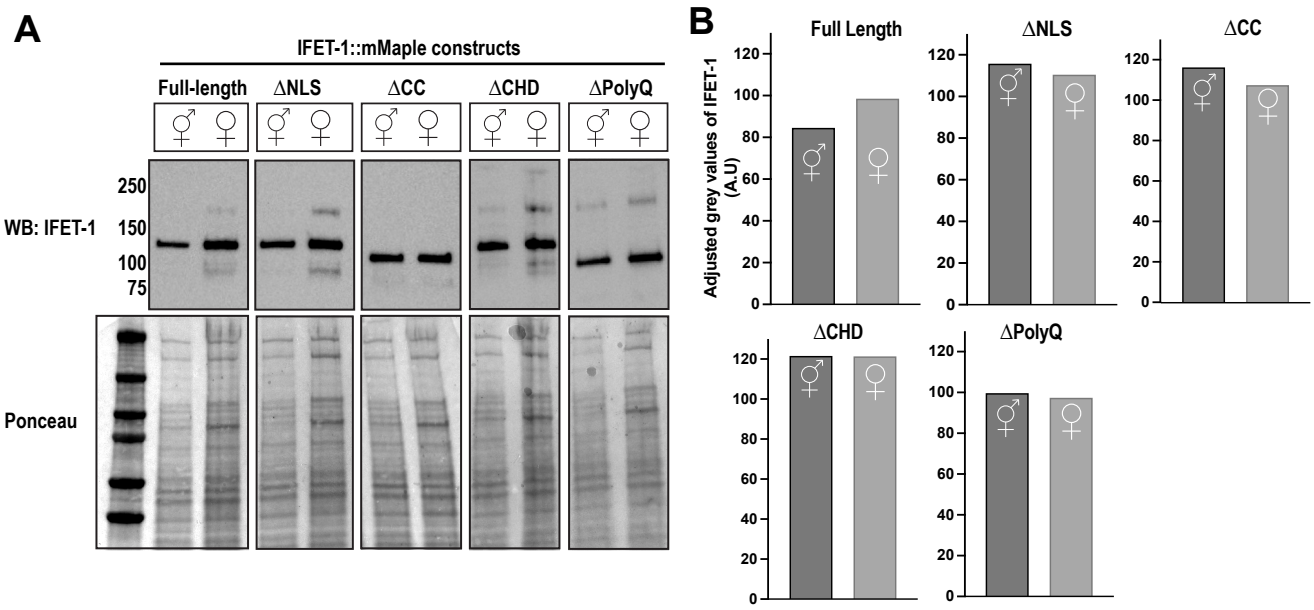
A
IFET-1::mMaple constructs
Full-length
ΔNLS
ΔCC
ΔCHD
ΔPolyQ
♂ ♀
WB: IFET-1
250
150
100
75
Ponceau
B
Full Length
ΔNLS
ΔCC
ΔCHD
ΔPolyQ
Adjusted grey values of IFET-1 (A.U)
0
20
40
60
80
100
120

Figure S3

A

Comparison of proteomics and transcriptomics

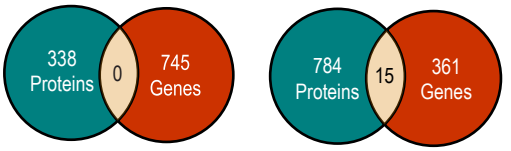

B

Proteins and genes that were down-regulated significantly in ifet-1(RNAi) worms

puf-5----------pumillo containing family
ifet-1----------eIF4E Transporter
clec-87----------C-type Lectin
wdfy-2----------WD40 and FYVE domain
cec-7----------chromodomain protein
acs-2----------fatty Acid CoA Synthetase family
pygl-1----------PYGL glycogen phosphoylase
tbb-1---------- tubulin beta
ddo-2---------- D-aspartate oxidase
lys-7---------- Lysozyme
ugt-26----------UDP-Glucuronosyl Transferase
cyp-34a9----------Cytochrome P450 family
C01G10.7
CELE_F32D8.12
Y52B11A.8

C

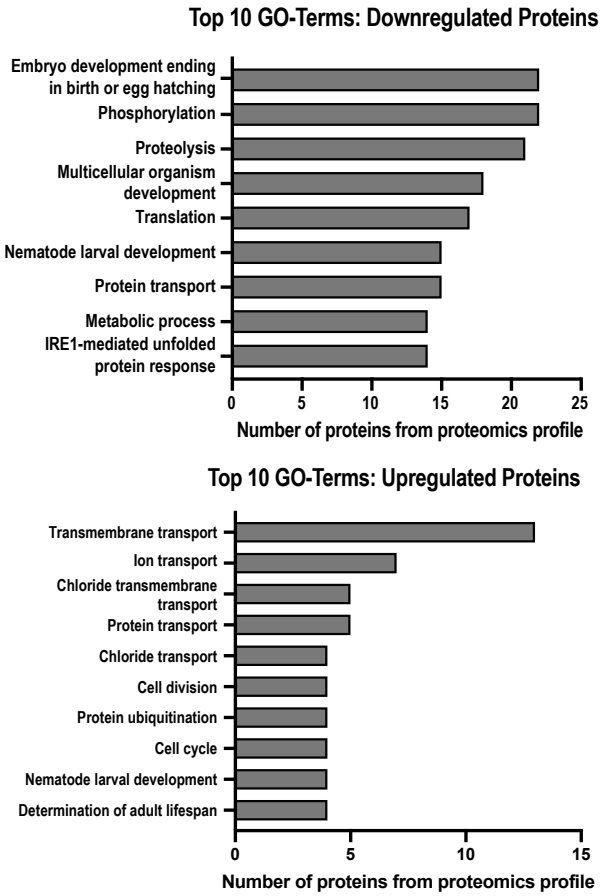

D

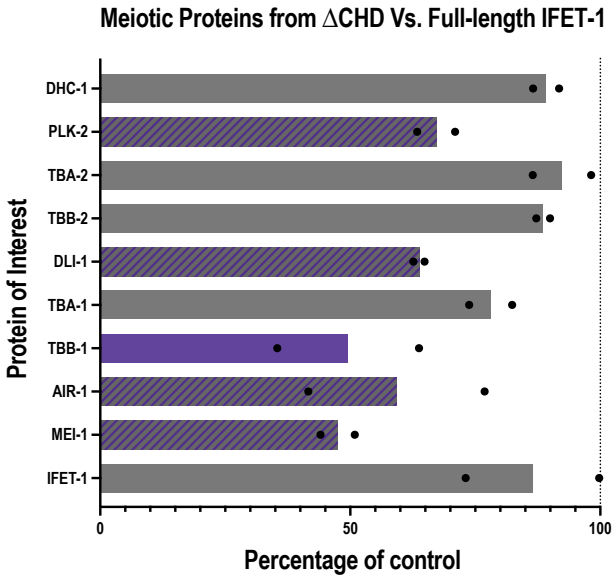

E

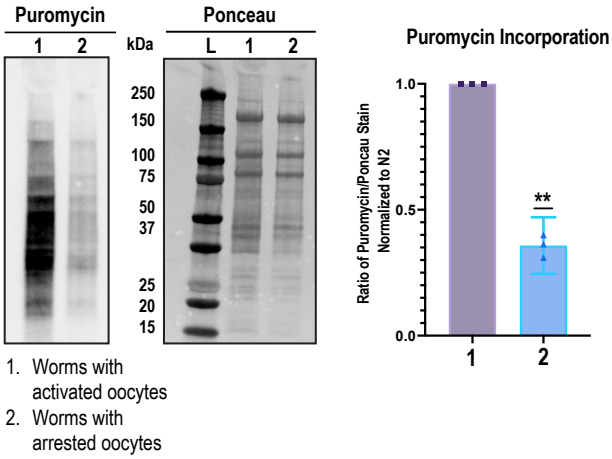

1. Worms with activated oocytes
2. Worms with arrested oocytes